https://doi.org/10.15407/ufm.20.04.584

T.G. JABBAROV, O.A. DYSHIN, M.B. BABANLI, and I.I. ABBASOV
Department of Mechanical and Materials Science Engineering,
Azerbaijan State Oil and Industry University,
16/21 Azadliq Ave., AZ-1010 Baku, Azerbaijan

MATHEMATICAL MODELLING OF THE SINTERING PROCESS OF IRON-BASED METAL-GLASS MATERIALS

Based on the study of the mechanisms of diffuse coalescence and coagulation, we review mathematical methods of description and construction of models for sintering process of the metal–ceramic materials. These models are represented by a set of nonlinear differential equations including bulk, grain-boundary, and surface diffusion coefficients, and correspond to a sequence of the temperature stage levels increasing with a certain rate and having different durations. By adjusting the levels, rates and durations of temperature regimes, technical parameters of the charge, it is possible to control the sintering process online. The description of the kinetics of liquid-phase sintering under pressure is performed based on the rheological theory of sintering using the diffusion–viscous flow mechanism. According to this mechanism, there are a tangential slippage along the grain boundaries and a decrease of the volume of pores due to the ejection of vacancies to the surface. After the formation of the liquid phase during sintering of the powder solid, (generally) firstly, there is a growth of grains, and then, a compaction of the obtained alloy. The process of sintering of the iron, cast iron, and sitall (glassceramic) powders is considered as the mutual diffusion of two (quasi)binary alloys: cast iron (iron + carbon) and fayalite (iron + sitall). The calculation of the interdiffusion coefficient of the resulting alloy is carried out according to the Darken formula. A number of features characterize sintering of multicomponent systems. The sintering of dissimilar materials (with different melting points) is a complex eutectic process, in which, along with self-diffusion, causing the mass transfer to the region of particle contact, there is an interdiffusion, which provides homogenization of the composition *via* equalization of the concentrations of dissimilar atoms within the sample. Under conditions of limited solubility or complete insolubility of the components,

sintering of the system is complicated by isolating homogeneous particles from mutual contact, hindering the flow of self-diffusion, and thereby, worsening the sintering conditions. For the numerical solution of the problem, a fourth-order Runge–Kutta method with a variable integration step is used. A software package for solving the problem is developed, the calculation results are given on the example of an alloy of a powder mixture of iron, cast iron, and sitallized glass.

Keywords: metal-ceramic and metal-glass materials, solid- and liquid-phase sintering, self- and interdiffusion, sintering rheology.

1. Introduction

The last decades are characterized by progress in the field of creating new types of powder materials with enhanced tribological properties that cannot be obtained by casting. Sintering can be called as one of the main technological operations of powder metallurgy. The complexity and versatility of the physical and physicochemical processes occurring during sintering make this problem one of the actual, albeit difficult, in the materials science.

The searches for ways to improve wear resistance led to the creation of iron-based materials with filling the pores by a sitallized glass. Solid inclusions of glass play the role of solid load-bearing inclusions held by a metal plastic matrix. The resulting metal-glass (MG) materials differ from their analogues with increased wear-resistance and low friction coefficient.

High brittleness of glass does not adversely affect the performance characteristics of products obtained from MG materials since small inclusions of glass melted and fill the pores during sintering are less susceptible to brittle fracture than large ones [1–7].

Antifriction properties of iron graphite with a pearlite-ferritic structure containing 6 vol.% of glass are studied. It is shown that the material containing glass has a lower coefficient of friction, less wear and a longer service life [8–11]. However, with a high demand for MG materials, they remain poorly understood.

To improve the interfacial interaction and the intensification of diffusion phenomena, and, consequently, increase the mechanical properties and wear resistance of iron-glass materials, they have to be alloyed with components more wetted by glass [12]. This effect can be caused, *e.g.*, by the use of cast iron powder in the composition of the charge, since cast iron contains a relatively larger amount of silicon and manganese, which have the property of formation of difficult-to-recover oxides when heated. It should be expected that these oxides in the sintering process will be well moistened with glass and thus contribute to its strong connection with the metal base. As a result of the studies in Refs. [13, 14], the best composition of the 'iron–cast iron–glass' powder

mixture is established to reach highest hardness and strength: 44% of iron, 50% of cast iron, and 6% of glass. We can consider the 1200 °C as an optimum sintering temperature for 'iron–cast iron'-type materials.

There are there stages of the sintering [15–17]: (i) temperature increasing — heating (non-isothermal, solid-phase sintering); (ii) exposure at a constant temperature (isothermal, liquid-phase sintering); (iii) temperature decreasing — cooling.

Solid-phase sintering of the powder solid is carried out by the diffusion mechanism and occurs without the formation of a liquid phase. At that, the following main processes occur: bulk and surface diffusion of atoms, compaction, recrystallization of the metal powder solid (growth of some grains due to others of the same phase), and the transfer of atoms of matter through the gas phase due to the bulk and surface diffusion, viscous flow caused by external loads during sintering under the pressure. This type of sintering is accompanied by the impact and development of bonds between particles (diffusion along grain boundaries and phases), the formation and growth of contacts (necks), the 'healing' of pores (closing through porosity) with their enlargement by spheroidization, compaction of the workpiece and its compaction. The latter occurs during heating and is mainly due to the bulk deformation of particles, carried out with bulk self-diffusion of atoms and adsorption of atoms (adatoms) on the surface (surface diffusion).

The fundamental works [18–22] are devoted to the description of the process of solid-phase sintering of metal solids, including powder ones. The theory of solid-phase sintering was further developed in the works [23–39] and others.

While the processes of the sintering of metal powders occurring in the solid phase are studied in detail (currently, there are theories explaining these processes), the sintering in the presence of the liquid phase is poorly studied. The presence of a liquid phase in the sintered system leads to a number of additional phenomena as compared with sintering in the solid phase, *e.g.*, processes of dissolution of the solid phase in the liquid and then solidification of the solid components, viscous flow of the liquid, *etc*. [40].

Some regularities of sintering in the presence of the liquid phase were firstly formulated in Refs. [41, 42], where the sintering process in the W–Ni–Cu system was investigated. Authors [41, 42] showed that the compaction during sintering is carried out in three stages. The first stage consists in the liquid flow towards the rearrangement of grains of the solid phase in the direction of their denser packing. The second involves the dissolution of small particles and the supercooling of the material on larger grains. The third phase may also include an additional compaction due to the coalescence of the grains between themselves, which has to obey the laws of sintering in the solid phase. Devel-

oping these ideas in Ref. [43], author presented theoretical calculation to the formula describing the processes of compaction during sintering for the first two stages. Authors of Refs. [44, 45] considered sintering with the liquid phase from the point of view of surface phenomena and gave an analysis of their quantitative laws.

Further development of the theory of sintering with a liquid phase was obtained in the works [46, 47], where authors stressed on the main differences occurring during sintering in liquid and solid phases. Along with the manifestation of capillary forces in the contact of particles (wetting and spreading of the liquid in solid particles, capillary pressure, penetration of liquid into the capillary slots between solid particles), the surface area of interaction between the components increases substantially. This dramatically accelerates the process of alloy formation and leads to the immeasurable manifestation of the associated thermal and bulk effects.

The diffusion-caused processes in alloys based on different types of crystal lattice (*e.g.*, f.c.c. [48, 49], b.c.c. [50] or h.c.p. [51, 52]), especially nanocrystalline (NC) and nanostructured (NS) alloys, are intensively studied and developed. This is because diffusion processes play an important role in the tuning properties of the materials, including processes of degradation and return of the form and structure of nanomaterials. In a number of experimental studies it was found that at a diffusion along the grain boundaries (GB) in NC and NS metals and alloys, the grain-boundary diffusion coefficients are several orders of magnitude greater than those in coarse-grained materials [29–30, 37].

The goal of this review work is the construction of mathematical models for porosity and graininess during sintering of a multicomponent mixture of powders of metal and ceramic materials. These models are represented by a closed system of differential equations corresponding to a sequence of temperature–time sintering regimes increasing with a certain rate. The scientific basis of the models are the mechanisms of diffusion coalescence kinetics and coagulation, occurring in a dispersed medium [53–57] and the rheological basis of pressure sintering kinetics using diffusion viscous flow mechanisms and heterodiffusion (interdiffusion) in alloys [23–24, 28, 46–47, 58–61]. Continuous 'fitting' of solutions at the joints of coupled temperature regimes is carried out using a specially developed set of computer programs for construction (Runge–Kutta-method-based) numerical solutions of a system of differential equations (at all temperature stages of sintering) with variable integration step. The results of calculations are presented on an example of solid-phase sintering of the pressed briquettes of a mixture of metal powders (iron and cast iron) containing sitallized, high-silicon-earthy glass powder of low concentration. The sintering process of this mixture is considered as mutual diffusion of two binary alloys: iron +

+ carbon (grey cast iron) and iron + sitall (metal-glass material Fe_2SiO_4, known as fayalite [62]). The coefficient of mutual diffusion in binary systems is calculated taking into account the Darken relation [63, 64].

The mathematical models available in the literature and methods for describing the kinetics of sintering processes of powder materials mainly scoped on one or two component systems [1, 3, 27, 65–70, 71, 72]. Sintering processes and their computer simulation for multicomponent systems consisting of several metal and ceramic powder and glass materials are studied not enough due to difficulties in the calculations of the interdiffusion coefficients [73, 74–78].

2. Theoretical Technique

2.1. Solid-Phase Sintering Kinetics of Powder Materials

During the period of rapid temperature rise, used before the isothermal treatment of active powders in the sintering process, a considerable compaction is commonly achieved with rates much higher than the rate after transition to isothermal (liquid phase) sintering.

For the mathematical description of compaction, the choice of the dependent variable becomes crucial. As such a dependent variable, author of Ref. [25] suggested to use the relative volume of pores υ_c/υ_n, where υ_n and υ_c are the pore volumes and solid porosity before and after sintering.

As follows from Ref. [28], during sintering of solids with different densities, values of the ratio of porosity of solids Π_c/Π_n after and before sintering (Π is a porosity defined as a fraction of the volume of the porous solid) are similar. At a significant change of the density of the porous solid before sintering, d_n [g/cm^3], the Π_c/Π_n ratio cannot be constant during the sintering process, which follows from the dependencies:

$$\upsilon_c/\upsilon_n = [d_n(d_k - d_c)]/[d_c(d_k - d_n)], \quad (1)$$

$$\Pi_c/\Pi_n = (d_k - d_c)/(d_k - d_n), \quad (2)$$

where d_c is sintered solid density, d_k is density of a compact matter (without pores).

From Eqs. (1) and (2), we find that

$$(\upsilon_c/\upsilon_n)/(\Pi_c/\Pi_n) = d_n/d_c. \quad (3)$$

From Eq. (2), after simple algebraic transformations, we obtain the following relation between the porosity Π_c and the volume shrinkage (compaction) $\Delta V/V_0$:

$$\Pi_c = 1 - (1 - \Pi_0)/[1 - (\Delta V/V_0)^2]. \quad (4)$$

The theoretical relationship between the volume shrinkage $\Delta V/V_0$ and the maximum value of interparticle contacts for sintering for sin-

tering powders achieved by sintering is obtained based on analysis of the geometry of the near-contact zone. When sintering by the mechanism of bulk or surface self-diffusion, the formation of contact is not accompanied by the convergence of particles, *i.e.* volume shrinkage in this case is absent. If the sintering is carried out due to a viscous flow or diffusion of vacancies in the contact of the boundary, capable of absorbing vacancies indefinitely, then the following relation between the relative approach of the particles is obtained, *i.e.* linear shrinkage $\Delta l/l_0$ and bulk shrinkage $\Delta V/V_0$ [28]:

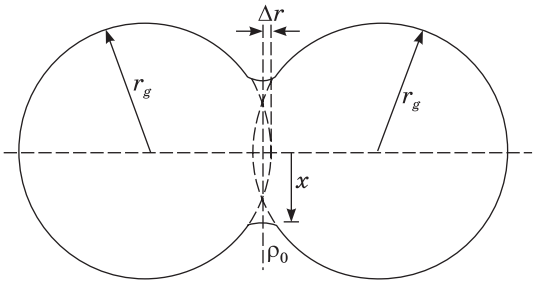

Fig. 1. Scheme of the idealized sintering model of two spheres [79]

$$\Delta V/V_0 = 3\Delta l/l_0. \quad (5)$$

In idealized sintering kinetics models, it is commonly assumed that any one mass transfer mechanism works during sintering and that mass transfer occurs at the point of contact between two identical spheres. However, we have to mean that during sintering of real samples, particles can have different shapes and sizes, each particle contacts several particles at once, contact in practice is not perfect (point), and in places of contact particles are usually flattened during compaction. However, most importantly, mass transfer in real samples is not controlled by any single process, but by several.

The initial stage of sintering is characterized by the formation and growth of the neck between the particles, followed by shrinkage of the sample, except the cases when mass transfer occurs only due to evaporation/condensation or bulk and surface diffusion. Shrinkage in the initial stage of sintering reaches only a few percent and occurs as long as the pores in the sample are almost completely interconnected and penetrate the entire volume.

Authors of Ref. [79] attempted to determine the parameters of grain-boundary diffusion by measuring shrinkage at the initial stage of sintering, based on a simplified model of sintering of two spheres (Fig. 1) with modified equations to describe the geometry of the resulting neck. In the works [19, 80, 81], the following relations were assumed to be satisfied:

$$\Delta r = \rho_0 = x^2/4r_g, \quad (6)$$

where Δr is approach of the centres of particles, ρ_0 is the radius of curvature of the surface of the neck, r_g is the radius of the particle.

In the paper [79], there were proposed modified equations for the shape of the neck, the distance between the centres of approaching par-

ticles Δr and the neck radius x:

$$x = (5\pi/9)r_g(\Delta r/r_g)^{0.46},\ \rho_0 = (7\pi/8)r_g(\Delta r/r_g)^{0.5}. \quad (7)$$

Using the geometric relations (7) and assuming that

$$\Delta l/l_0 = \Delta r/r_g, \quad (8)$$

they obtained equation for shrinkage kinetics [79]:

$$\Delta l/l_0 = (50\gamma\Omega bD_b/7\pi k_B T r_g^4)^{0.31} t^{0.31}, \quad (9)$$

where γ is surface tension associated with surface pressure σ (also called capillary pressure) in the case of a spherical particle of radius r_g by ratio $\sigma = 2\gamma/r_g$, b is the width of the boundary between the particles, k_B is the Boltzmann constant, T is the absolute temperature, Ω is the atomic volume.

From Eq. (9), it follows that the diffusion permeability of grain boundaries (bD_b) can be determined from the slope of the shrinkage curve (*i.e.*, the dependences $\Delta l/l_0$ on $t^{0.31}$):

$$bD_b = [-\partial(\Delta l/l_0)/\partial t^{0.31}]^{1/0.31}(7\pi k_B T r_g^4/50\gamma\Omega). \quad (10)$$

It should be noted that Eq. (10) is valid only for $x < 0.3r_g$ or close to this inequality, since it is assumed that the equation for the driving force in [79] assumed that $x \le r_g$.

There was shown [35] that the geometry of the neck, described by Eq. (7), is still far from the exact formula obtained by numerical methods. It was assumed that the mutual penetration of the spheres that the volume of the lenticular area of overlapping spheres is equal to the newly formed volume around the point of contact. However, this assumption is exactly fulfilled if there are no transfer mechanisms that do not shrink (*e.g.*, surface diffusion and evaporation or condensation).

The paper [82] deals with analysis of the mass transfer with an account of grain-boundary and bulk diffusions, where authors suggested improved equations of the geometry of the neck obtained dynamically (without using the graphical method):

$$x = 1.92r_g(\Delta r/r_g)^{0.49},\ \rho_0 = 2.32r_g(\Delta r/r_g)^{1.14}. \quad (11)$$

The final shrinkage equation, based on relations (11), has the form:

$$(\Delta l/l_0)^{2.1}\left[d(\Delta l/l_0)/dt\right] = \frac{2\gamma\Omega D_V}{k_B T r_g^3}\frac{\Delta l}{l_0} + \frac{\gamma\Omega bD_b}{2k_B T r_g^4}. \quad (12)$$

From the last formula, it follows that the curve of shrinkage kinetics in the coordinates $(\Delta l/l_0)^{2.1}[d(\Delta l/l_0)/dt]$ and $\Delta l/l_0$ should be a straight line, the slope of which gives the coefficient diffusion D_V, and the segment cut off from the ordinate axis bD_b is the product for grain boundary diffusion.

The most complete description of the sintering model of two spheres, which takes into account both the energy of grain boundaries and its

effect on the neck surface, and additional volumetric diffusion from the neck surface, was given in [33], where exact solutions were used to describe the neck geometry. For this, along with ρ_0, the parameter A_r was introduced, which is the area on the neck surface, which atoms can achieve through bulk diffusion.

$$A_r = 4\pi\rho_0[(C - (\pi - B)/2)(r_g + \rho_0)\cos C - \rho_0(\sin C - \sin((\pi - B)/2))], \quad (13)$$

where

$$C = \sin^{-1}[r_g - \Delta r + \rho_0 \sin((\pi - B)/2))/(r_g + r_0)]. \quad (14)$$

In the last two expressions, B is the angle of the solution of the grain-boundary groove in the neck between the particles, which is formed to achieve local equilibrium between the surface tension of the grain boundary and the free surface of the neck.

Assuming again the valid relation (8), the author obtained the following equation of shrinkage kinetics [33]:

$$[X^3\rho_0/(r_g X + \rho_0 \cos((\pi - B)/2))]d(\Delta l/l_0)/dt =$$

$$= (2\gamma\Omega D_V/\pi k_B T r_g^3)XA_r/r_g^2 + 4\gamma\Omega b D_b/k_B T r_g^4, \quad (15)$$

where $X = x/r_g$ is a specific neck size. It did not take into account the existence of transfer mechanisms that did not contribute to shrinkage (such as surface diffusion and transfer through the gas phase).

As follows from (15), measuring the shrinkage rate, the neck size and the angle of the groove solution located in the neck at the grain boundary, one can obtain as a result of sintering experiments the values of the coefficients of volume and grain boundary diffusion by constructing the dependence $[X^3\rho_0[d(\Delta l/l_0)/dt]/[r_g X + \rho_0 \cos((\pi - B)/2)]$ from $A_r/r_g^2 X$. This results in a straight line with a slope λ, giving the coefficient of bulk diffusion D_V, and a segment K, cut off on the axis $A_r/r_g^2 = 0$, giving the product bD_b for grain boundary diffusion:

$$D_V = (\pi k_B T r_g^3/2\gamma\Omega)\lambda, \; bD_b = (k_B T r_g^4/4\gamma\Omega)K. \quad (16)$$

If there is no mass transfer from the surface, then, Eq. (15) becomes simpler and takes the form

$$(\Delta l/l_0)^{2.06}\frac{d(\Delta l/l_0)}{dt} = \frac{2.63\gamma\Omega D_V}{k_B T r_g^3}(\Delta l/l_0)^{1.03} + \frac{0.70\gamma\Omega b D_b}{k_B T r_g^4} \quad (17)$$

for the first 3.5% of shrinkage. Expression (17) only slightly differs from Eq. (12), obtained by neglecting surface diffusion and bulk diffusion from the surface, as well as using the approximation of expression (11) for the geometry of the neck.

If the bulk diffusion D_b dominates over the grain boundary diffusion D_b, Eq. (17) has a solution with respect to $y = \Delta l/l_0$:

$$y \cong (5.34\gamma\Omega D_V/k_B T r_g^3)^{0.49} t^{0.49}. \quad (18)$$

In the opposite case, when grain-boundary diffusion dominates over bulk diffusion, equation (17) has the solution:

$$y \cong (2.14\gamma\Omega bD_b/k_BTr_g^4)^{0.33}t^{0.33}. \quad (19)$$

Denoting $y = \Delta l/l_0$ and substituting (5) in (4), we obtain an equation, which relates Π_c/Π_0 with $\Delta l/l_0$:

$$\Pi_c = 1 - \frac{1-\Pi_0}{(1-3y)^2}.$$

Solving this equation for y, we obtain

$$y = \frac{1}{3}\left[1 - \left(\frac{1-\Pi_0}{1-\Pi_c}\right)^{1/2}\right].$$

Differentiating with respect to t both sides of the equation for Π_c and taking into account the expression for y, we obtain

$$\frac{d\Pi_c}{dt} = -\frac{6(1-\Pi_c)^{3/2}}{(1-\Pi_0)^{1/2}}\frac{dy}{dt}. \quad (20)$$

The last equation can now be written as

$$\frac{d\Pi_c}{dt} = -\frac{6(1-\Pi_c)^{3/2}\cdot 3^{2.1}}{\sqrt{1-\Pi_0}\left[1-\sqrt{\frac{1-\Pi_0}{1-\Pi_c}}\right]^{2.1}}\left\{\frac{2\gamma\Omega D_V}{3k_BTr_g^3}\sqrt{\frac{1-\Pi_0}{1-\Pi_c}} + \frac{\gamma\Omega bD_b}{2k_BTr_g^4}\right\}. \quad (20')$$

For the first 3.5% of shrinkage, we will use the kinetic equation (17), which can be written, taking into account the above relation Π_c with y, as a differential equation:

$$\frac{d\Pi_c}{dt} = \frac{-6(1-\Pi_c)^{3/2}\cdot 3^{2.06}}{\sqrt{1-\Pi_0}\left[1-\sqrt{\frac{1-\Pi_0}{1-\Pi_c}}\right]^{2.06}}\left\{\frac{2.63\gamma\Omega D_V}{3^{1.03}k_BTr_g^3}\left[\sqrt{\frac{1-\Pi_0}{1-\Pi_c}}\right]^{1.03} + \frac{7\gamma\Omega bD_b}{10k_BTr_g^4}\right\}. \quad (20'')$$

For a topologically continuously transforming structure of a powder material in the sintering process, a quantitative analysis of the kinetics of changes of the characteristic linear parameter of the porous microstructure L (L is an average grain size of the sample) can be performed using the general theory of diffusion coalescence of disperse systems [83]. If the main mechanism of mass transfer is a surface diffusion, then kinetic equation for L (dependent on time t) is [84]:

$$L^4 = L_0^4 + (B_1\gamma D_S\delta^4/(k_BT))t, \quad (21)$$

where D_S is the surface diffusion coefficient, $\Delta L = L - L_0$ is the thickness of the layer, where surface diffusion takes place, of the order of atomic diameter δ, γ is the surface tension, B_1 is a numerical constant ≈ 30, L_0 is the initial value of L before the sintering.

The last equation satisfies many experimental data for oxide and metal powders [32, 35, 84]. For metal island-type films, the coalescence occurs predominantly *via* the mechanism of surface diffusion of adatoms [22, 85].

Differentiating (21) with respect to t, we obtain the kinetic differential equation for L:

$$dL/dt = B_1 \gamma D_S \delta^4/(4L^3 k_B T). \qquad (22)$$

2.2. Iron Self-Diffusion and Carbon Diffusion in Iron

The subject of our consideration is the diffusion mechanism of sintering a powder mixture, which is based on iron (44%) and grey cast iron (50%). Depending on the grade, the composition of grey iron includes C (2.9–3.7%), Si (1.2–2.6%), Mn (0.5–1.1%), P (more than 0.2–0.3%), and S (0.12–0.15%). There is permission for alloying grey cast iron with Cr, Ni, Cu, and some other components.

Generally, the diffusion coefficient D, which is an important quantity that determines the diffusion rate, depends on the nature of the alloyed and alloying atoms (see, *e.g.*, Refs [86–88]) as well as the structural factors (grain size, density and distribution of lattice defects), but most strongly depends on temperature. The dependence of the diffusion coefficient D on temperature obeys the Arrhenius law [89, 90]:

$$D = D_0 \exp(-\Delta H/(k_B T)) \qquad (23)$$

or

$$D = D_0 \exp(-Q/(RT)), \qquad (23')$$

where R is a universal gas constant, D_0 is a pre-exponential factor different from the value of D_0 in Eq. (23), Q is the activation energy. Dependence (23) is experimentally confirmed for many systems with high D for diffusion in interstitial alloys (*e.g.*, carbon in α- and γ-Fe) and substitution alloys (*e.g.*, Au in Ag).

The exponential temperature dependence of D is explained by the origin of diffusion due to thermally activated atomic motion, which is always described by the exponential $\exp(q/k_B T)$, where q is the activation energy of the elementary act of atom displacement.

Table 1 [89] contains characteristics of the parameters of self-diffusion of ferrite or α-iron (Fe below 912 °C), and austenite or γ-iron (Fe above 912 °C); while Table 2 [89] exhibits carbon diffusion coefficient in them. The activation energy of self-diffusion of metals ΔH_D relates to the melting temperature T_m: $\Delta H_D/T_m \simeq 1.5 \cdot 10^{-3}$ eV/K and the ratio $\Delta H_D/T_m \simeq 15$ with the heat of fusion L_h. These empirical rules allow us to estimate the value of the diffusion coefficient in the case of the measurement impossibility. However, there are some exceptions, *e.g.*, for Ge.

Atoms in austenite are arranged into an f.c.c. crystal structure. Heating the ferrite up to 912 °C leads to the formation of the smallest austenite grains at the boundaries of ferritic grains. Further heating leads to the growth of new austenitic grains with the complete replacement of old ferritic grains with new austenitic ones — transformations occur in iron: the crystalline structure of iron spontaneously transforms from b.c.c. into f.c.c. At the cooling below 912 °C, transformations of the same type occur in Fe but in the opposite direction.

The activation energy Q is expressed in terms of the activation enthalpy ΔH [89],

$$Q = \Delta H + RT, \tag{24}$$

and obeys the Arrhenius law [91],

$$r = A\exp(-Q/RT), \tag{25}$$

where r is the reaction rate for sum of reactants $A_1 + A_2$ to be converted into product A_1A_2, A is a pre-exponential factor.

The activation energy Q and pre-exponential factor A can be calculated from the experimental data [91]. Consider an elementary second-order reaction in which two different particles $A_1 + A_2 \rightarrow$ products with different concentrations of the substance A_1 and A_2. We assume that with an excess of A_2, the order of reaction for substance A_2 is zero. Then, the expression for the rate of this reaction has the form $-dc/dt = rt$. Integrating the right side of this equation in the range $[0, t]$ and the left one in the range $[c_0, c]$ allows calculating the chemical reaction constant r:

$$r = (1/t)\ln(c_0/c), \tag{26}$$

where c_0 is the initial concentration of the initial reactant A_1 at the moment of time $t = 0$, c is the concentration of this reactant at the moment of time t.

Table. 1. **Diffusion coefficient of iron [89]**

Self-diffusion in pure metals					
Metal	Structure	D_0, cm^2/s	ΔH_D, eV	$\Delta H_D/T_m$, eV/K	$\Delta H_D/L_h$
α-Fe	b.c.c.	2	2.5	$1.4\cdot10^{-3}$	15.5
γ-Fe	f.c.c.	0.4	2.8	$1.6\cdot10^{-3}$	17.4

Table 2. **The diffusion coefficient of carbon in ferrite and austenite [89]**

Impurity diffusion in metals					
Type of solution	Metal	Impurity	D_0, cm^2/s	ΔH, eV	D/D^* at 1000 K
Interstitial solid solution	α-Fe	C	0.004	0.83	$1.44\cdot10^6$
	γ-Fe	C	0.67	1.6	$3.87\cdot10^6$

From Eq. (25), we obtain

$$Q = [R(T_2T_1)/(T_2 - T_1)]\ln(r_2/r_1), \tag{27}$$

where

$$r_j = (1/t_j)\ln(c_0/c_j)\ (j = 1, 2). \tag{28}$$

Two different formulas (23) and (23′) for diffusion coefficient yield

$$\Delta H/Q = k_B/R, \tag{29}$$

which results to

$$\Delta H = Q/N_A, \tag{30}$$

where the relation $k_B = R/N_A$ (N_A — Avogadro's number) is used.

Sometimes, there is a deviation from the Arrhenius equation, which can be interpreted as inconstancy of the (effective) reaction activation energy at different temperatures.

To determine experimentally the distribution of the A diffusant concentration in a substitutional solid solution B (in our case of a cast iron, A — graphite, B — iron), a diffusion pair (bi-pair) is applied. It consists of two semi-infinite samples (A and B) interconnected by a flat boundary through which diffusion occurs from one sample (A) with an initial diffusant concentration c_2 to another sample (B) with an initial diffusant concentration c_1 ($c_1 < c_2$).

From a practical point of view, to obtain the distribution of the carbon concentration in iron, the most important is to build the distribution of carbon concentration after the so-called cementation (surface saturation of the material with carbon) [92]. Commonly, the cementation is carried out at 910–950 °C, and sometimes to accelerate the process — at 1000–1050 °C, *i.e.* at the temperature of chemical heat treatment (CHT), the diffusion zone at any time moment has an austenitic structure with a variable concentration of carbon, decreasing with distance from the surface into the depth of the product.

In the surface layer of the product, the carbon concentration is usually 0.8–1.2 mas.% and does not reach the limit of solubility at the carburizing temperature. Therefore, the Fe_3C is not formed at this temperature, and the surface layer (as well as in the bulk) is in the austenitic state. The transformation of ferritic grains into austenitic ones occurs as follows. When ferritic iron is heated to 912 °C, the old composition of ferritic grains changes to a new composition of austenitic grains, *i.e.* α-iron transforms into β-iron. Firstly, there is a formation of new, very fine, austenitic grains, which overlap old boundaries of ferritic grains thereby forming the so-called perlite. Then, these grains grow until all the old ferritic grains disappear and cementite appears. Transformation of the ferrite into austenite is accompanied with volume changes. The density of austenite is 2% higher than that of ferrite;

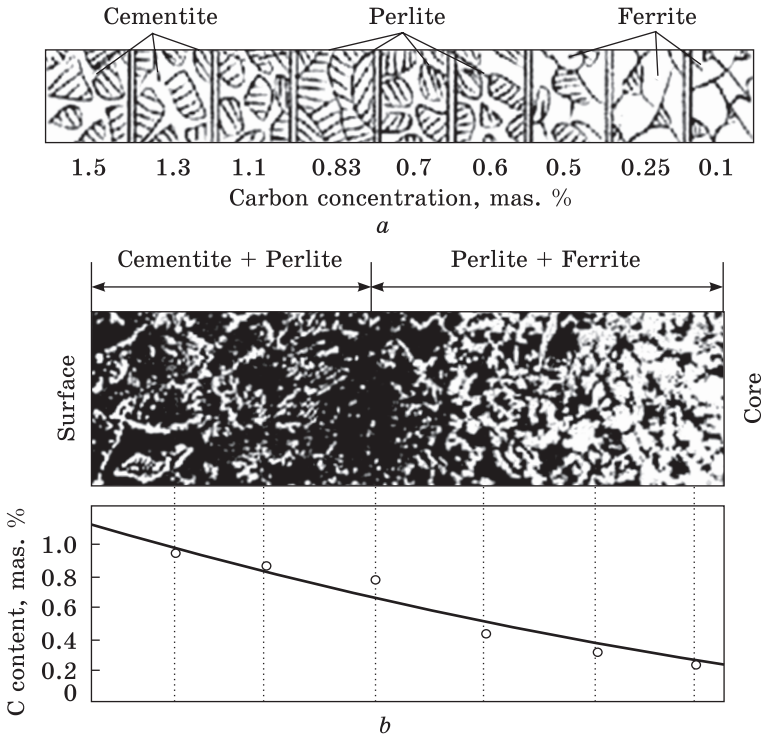

Fig. 2. Plotting the carbon concentration distribution after cementation according to optical microscope data [64]

it means that the austenite atom occupies a smaller volume than the ferrite atom [93].

On the region of the diffusion zone adjacent to the surface, and having a carbon concentration more than 0.8 mas.%, at room temperature, there is cementite + perlite; while the region with a carbon concentration less than 0.8 mas.% is occupied by excess ferrite + perlite (Fig. 2, *a*), [92]). Moving from the surface, due to the continuous decreasing of C concentration, secondary cementite gradually disappears, and the structure becomes pure pearlitic, and then the amount of pearlite gradually decreases and the volume fraction of ferrite increases.

Thus, at a high CHT temperature, the diffusion zone (cemented layer) is a single-phase; after slow cooling, it becomes a two-phase (ferrite + cementite) over the whole section. Observing the surface structure of carburized iron (*e.g.*, *via* an optical microscope), using the relation for different structural components, one can approximately construct the distribution of the carbon concentration c_C (Fig. 2, *b*) [92]).

When the liquid metal, obtained after the melting temperature T_m (for Fe, T_m = 1540 °C), is cooled to the point of solidification, then, when

a liquid state transforms into a solid one, a phase transformation occurs between the liquid and the solid phases with a heat release. When cooling the austenite it transforms into ferrite, it is also a phase ($\gamma \rightarrow \alpha$) transformation; however, in this case, the solid state transforms into the solid one (also with a heat release). In case of a heating, the opposite process occurs: α-phase of Fe transforms into the γ-phase (with heat absorption).

The cementation is an intermediate operation, followed by quenching (rapid cooling). The hardness of the resulting material is proportional to the final carbon content. After the quenching of the cementite, we can analyse the hardness over the sample cross-section, moving away from the surface to the sample centre. Using analysed experimental data, we can plot the functional dependence of hardness on the distance from the surface: the resultant hardness–distant curve acts as a concentration curve of carbon content in the alloy.

2.3. Application of Sitallized Glass: Main Advantages

Sitallized glass (the so-called sitall) is an artificial polycrystalline material, obtained by crystallization of glass of the appropriate chemical composition, possessing higher physicochemical properties as compared with this glass. 'sitall' is a combination of two words: 'glass' and 'crystal. One can say that sitall is something like hybrid of glass and ceramics. There are distinctions from glass and ceramics: (granular) crystalline structure and much smaller crystals with monolithic structure, respectively. An important stage of the transformation of glass into sitall is the formation of crystallization centres, which can occur spontaneously (homogeneous mechanism) or due to the introduction of foreign outer particles (heterogeneous nucleation) [94].

In a process of sintering of iron with sitall, a metal-glass material Fe_2SiO_4 is formed called as fayalite [95]. Moving over the metal, the molten sitall accumulates mainly in the grain boundaries, is saturated with metal absorbing its oxides, and crystallizes.

Metal-glass materials should be distinguished from amorphous materials, in which, unlike crystalline, there is no a long-range order in the arrangement of atoms. Such materials can be obtained by solidification of a drop of metal melts under conditions of intensive heat removal by the 'shooting method' and are called as amorphous metal alloys or metal glasses [96].

The nature of the properties of glass ceramics has much in common with the nature of the same properties of the original glass and similar ceramic materials, and at the same time significantly exceeds these indicators. Sitall is several times stronger than glass, most ceramic materials and even some metals, its bending strength can reach 2500–3000 kg/cm^2 and for some experimental samples — 4200–5600 kg/cm^2,

i.e. exceeds the strength of quartz glass, stainless steel, and titanium. Sitall has a dense microcrystalline structure similar to the structure of ceramic materials based on pure oxides, characterized by rather small sizes of randomly oriented crystals and the absence of porosity. For phosphate-containing sitall, crystal sizes range from 0.5 to 6 μm; while 20–50 μm for conventional ceramics. The density of sitall is 2.5–2.72 g/cm^3 providing indentation hardness close to the hardness of hardened steels and greater than the hardness of fused quartz, brass, cast iron, granite, and glass.

Iron-based metal-glass materials, as a rule, have a heterogeneous structure, contributing to the improvement of mechanical properties and wear resistance. The role of glass is that it wets the metal base, strengthening the metal frame by dissolving metal oxides in the glass. To intensify the processes of interfacial interaction, and as a result, increase the mechanical properties and wear resistance of iron-glass materials obtained by cold pressing and subsequent sintering, they have to be doped with well-wetted glass components. In this regard, it seems appropriate to use the iron powder as an alloying component of iron-glass materials.

For this purpose, we used grey cast iron, which (depending on the grade) includes C, Si, Mn, P, S. The presence of silicon and manganese contributes to the formation in the process of heating of the difficultly reducible oxides. It should be assumed that in the process of sintering, these oxides will be well wetted with glass and, to some extent dissolving in the glass, will promote adhesion of the metal frame to the glass.

The results of work [96, 97] show that in the microstructure of metal-glass composite materials, in particular, based on Fe, after sintering, in addition to the metal base, pores and inclusions of glass, a new phase such as fayalite and hematite may appear as a result of metal-glass interaction.

The study of the structure and properties of composite materials based on mixtures of iron and cast iron powder showed [99, 100] that an increase in the content of cast iron powder in the mixture leads to a slight increase in the porosity of the samples at the same pressing pressure. With decreasing particle size of cast iron powder, the density of compressed pellets increases and the value of elastic aftereffect decreases.

2.4. Pre-Exponential Factor of Diffusion Coefficient in the Fe-Alloy and Sitallized Glass

The observed values of the pre-exponential factor of diffusion coefficient D_0 for amorphous alloys have a much greater variation (10^{-15}–10^{15} m^2/s) than the corresponding values for crystalline alloys (10^{-6}–10^2 m^2/s) and, therefore, the values of D_0 for amorphous alloys and crystalline systems with the same ΔH can differ by several orders of

magnitude [101]. For the experimental values of D_0 and the enthalpy of diffusion activation ΔH of amorphous alloys, the following relation was established [102]:

$$D_0 = A e^{\Delta H/B}, \tag{31}$$

where A and B are constants. This relationship is universal in the sense that it satisfies not only amorphous alloys [103, 104], but also the D_0 value for self-diffusion and impurity diffusion of crystalline alloys, including displacements of atoms into the substitutional or interstitial lattice sites [105, 106].

The comparison of the values of the parameter A (10^{-7} m^2/s) for crystalline alloys with the corresponding values (10^{-19}–10^{20} m^2/s) for amorphous alloys and the values of B (0.41 eV) for crystalline alloys and (0.055 eV) for amorphous alloys shows that these parameters are absolutely different [107].

For the diffusion of vacancies or cracks in crystals, the constants A and B are calculated using the Zener theory for the pre-exponential factor [108]. According to this theory, the pre-exponential factor D_0' (identical to D_0 for crystals) reads as

$$D_0' = ga^2 f\nu_0 e^{\Delta S/k_B}, \tag{32}$$

where g — geometric factor, a — effective distance between atomic hops (jumps), ν_0 — effective frequency of jumps (hops), f — correlation factor, and ΔS — entropy of diffusion.

For crystals,

$$\Delta S = -\beta_\mu \Delta H, \tag{33}$$

where β_μ represents the temperature dependence of the shear modulus [104, 105]. As follows from Eqs. (32) and (33), A in Eq. (31) is

$$A = ga^2 f\nu_0,\ B = -k_B/\beta_\nu, \tag{34}$$

which is well confirmed by experimental data for the diffusion in crystals [104]. Using Eqs. (32)–(34) for crystals, we obtain

$$D_0 = ga^2 f\nu_0 e^{-\Delta H\beta_\mu/k_B}. \tag{35}$$

For metal systems, $a = 3\cdot 10^{-10}$ m and $\nu_0 \approx 10^{12}$ 1/s, we can assume $fg \approx 1$, so the parameter A is approximately equal to 10^{-7} m^2/s with a deviation for different metals no more than one order [104].

For crystals, the correlation dependence between D_0 and Q (as noted above, $Q \approx \Delta H$) was investigated previously in Ref. [109]. Using the thermodynamic approach there were obtained the expression

$$\Delta S \approx \beta_\mu Q, \tag{36}$$

where

$$\beta_\nu = -\partial(\ln\mu)/\partial T \tag{37}$$

is temperature dependence of the shear modulus. As a result, the following relationship was obtained for diffusion of crystals (so-called Zener

ratio):

$$\ln D_0 = \ln A + \beta_\mu Q/k_B; \quad (38)$$

particularly, $\beta_\mu \approx 2.2\cdot10^{-4}$ 1/K for Cu, Ni, Pd, while $\beta_\mu = 3.5\cdot10^{-4}$ 1/K for Ag [110].

Thus, the pre-exponential factor D_0 for metal alloys (in particular, for fayalite Fe_2SiO_4) can be determined by the formula

$$D_0 = A\, e^{-\Delta H\beta_\mu/k_B}, \quad (39)$$

where $A = 10^{-7}$ m_2/s for all metal alloys, and $\beta_\mu = 2.85\cdot10^{-4}$ 1/K is the characteristic (average) value of the parameter β_μ for metals.

Thus, the diffusion coefficient of Fe_2SiO_4 can be written as the Arrhenius formula (23) with a pre-exponential factor D_0 defined by formula (39), *i.e.*

$$D = A^{-\Delta H\beta_\mu/k_B} e^{-\Delta H\beta_\mu/(k_B T)} \quad (40)$$

with $A = 10^{-7}$ m^2/s and $\beta_\mu = 2.85\cdot10^{-4}$ 1/K. The value of activation enthalpy ΔH is calculated *via* the formula $\Delta H = Q/N_A$, and the activation energy Q (or E as denoted in Ref. [34]) is determined by formula (30).

In the works [102, 103, 111, 112], an attempt was made to establish a correlation dependence of $\ln D_0$ on Q for self-diffusion and impurity diffusion of amorphous alloys using formula (31) and the Zener's ratio with parameter $B = k_B/\beta\mu$. However, the value of $\beta_\mu = 1.6\cdot10^{-3}$ 1/K, thus obtained deviated from the known average values of elasticity by a value of approximately one order of magnitude [107]. This is explained by the fact that, under the conditions of boundary diffusion between clusters of a heterogeneous amorphous alloy, the values of the parameters A and β_μ strongly depend on the properties of the boundary region, which are unknown in most cases. Consequently, the correlation dependence of $\ln D_0$ on Q cannot be obtained using a relation similar to Eq. (36) in the case of amorphous alloys.

2.5. Calculation of Diffusion Coefficients from Experimental Data on Annealing

A systematic quantitative analysis of grain-boundary diffusion became possible only after the appearance of the article [113]. Almost all earlier works on grain boundary diffusion were qualitative, since they did not provide numerical data that serve as rigorous evidence of the true coefficients of grain boundary and bulk diffusion. However, even in that time it was clear that solutions of equations for bulk diffusion, corresponding to diffusion in an inhomogeneous medium, could not be directly used to determine the grain-boundary diffusion coefficients. This is because the process is heterogeneous and is complicated by the fact that diffusion along the grain boundaries is always accompanied by removal of diffusant from the boundaries to the bulk of grains, *i.e.* bulk diffusion appears with a coefficient of D_V.

As was suggested [113], the grain boundary is a thin homogeneous layer with a thickness δ of several interatomic distances in a semi-infinite crystal, and the grain-boundary coefficient diffusion D_b over this layer is much larger than the coefficient of volume diffusion D_V beyond its limits. This problem was solved [113] taking into account the removal of the diffusant from the grain boundary to the crystal bulk, but neglecting direct bulk diffusion from the diffusant source on the surface. As shown [113], if the grain-boundary diffusion dominates, the logarithm of the average concentration $\overline{c}$ in such a layer (parallel to the source of the diffusant) varies linearly with the depth of penetration z, in contrast to the parabolic dependence for bulk diffusion. However, this conclusion [113] was based on a set of approximations and was not exact. The exact solution of the same problem, *i.e.* for the model of a uniform layer at the grain boundary, was obtained in Refs. [114, 115] for diffusion from an 'instantaneous' source (an infinitely thin layer on the surface). Exact solution [114] for the model in Ref. [113] was too complicated for experimenters for using in practice.

Following above-mentioned theoretical works, another article [116] appeared where authors used completely different approach to grain-boundary diffusion based on the consideration of the entire polycrystalline solid. They showed that, in the region of grain-boundary diffusion, $\lg \overline{c}$ varies linearly not with z, but with $z^{6/5}$. Just after the work [116], experimenters had the opportunity for using exact solutions of the problem of grain boundary diffusion in order to process the obtained data.

The model of grain-boundary diffusion proposed in Ref. [116] although is far from reality, is quite suitable for describing experiments under certain conditions [37]. The grain boundary is a semi-infinite isotropic layer of the same thickness δ with a high diffusion coefficient (restricted in a semi-infinite perfect crystal with a low diffusion coefficient) with the grain boundary perpendicular to the surface on which there is a diffusant.

Let the y-axis be perpendicular to the grain boundary layer, and the z-axis perpendicular to the free surface. At the diffusion annealing of sample with a temperature T and annealing time τ, material diffuse along the z-axis into the bulk of the grain as well as along the grain boundary. The diffusion coefficient at the boundary is much larger than elsewhere, and therefore the bulk diffusion of matter begins from the walls of the grain boundary into the surrounding crystals. Let D_V be the bulk diffusion coefficient describing diffusion in the grains, and D_b be the diffusion coefficient in the grain boundary layer. If $D_b \gg D_V$, the direct diffusion contribution from the surface decreases with distance much faster than the grain boundary contribution. Therefore, in the region far from the surface, diffusant enters to the bulk practically from the grain boundaries only. The derivation of the diffusion equa-

tion is based on the following assumptions: (1) the diffusion laws are satisfied both in the crystal and in the grains; (2) the diffusion coefficients D_V and D_b are isotropic and do not depend on the concentration, coordinates and time; (3) the diffusant concentration $c(z,\tau)$ and its flux J_z in the z-direction, determined by the first Fick's law,

$$J_z = -D_V \partial c(z,\tau)/\partial\tau, \qquad (41)$$

are continuous on the walls of the grain boundary, *i.e.* at $y = \pm\delta/2$, at that, the flow J_z is continuous at the interface between the boundary and the grain; (4) the grain boundary thickness δ is so small that a change in the concentration across the boundary (*i.e.*, in the y-direction) can be neglected.

An approximate solution of the problem of grain-boundary diffusion for the case with a constant concentration source at $z = 0$ was obtained in Ref. [113], where the diffusant concentration in all other points of the system was assumed zero. The exact solution for diffusion from a source with a constant concentration was obtained in Ref. [114]. The solutions in Refs. [113, 114] are valid only for fine grain boundaries, when $D_b \gg D_V$, and when the diffusion coefficients D_b and D_V do not depend on concentration, coordinates, and time, and the condition of continuity of inflow on the interface between the grain boundary layer and the crystal is satisfied.

To describe the grain-boundary diffusion analytically, the dimensionless variables ε, η, β (corresponding to y, z, τ), and the dimensionless parameter Δ,

$$\varepsilon = \frac{y-\delta/2}{(D_V\tau)^{1/2}},\ \eta = \frac{z}{(D_V\tau)^{1/2}},\ \beta = \frac{(\Delta-1)\delta}{2(D_V\tau)^{1/2}} = \frac{\delta D_b}{2D_V^{3/2}\tau^{1/2}},\ \Delta = \frac{D_b}{D_V}, \qquad (42)$$

are introduced.

The physical meaning of the η parameter is in that it describes the influence of direct bulk diffusion from a source into a crystal at a given depth z: the stronger this influence, the lesser η. The parameter ε (dependent on a given distance from the plane of the grain boundary) describes the contribution of bulk diffusion from the grain boundary to the crystal. The parameter Δ shows how many times the diffusion along the grain boundaries is greater as compared to the bulk diffusion. At the solid-phase sintering, carried out at low and medium temperatures, the coefficient of grain boundary diffusion D_b is significantly greater than the coefficient of bulk diffusion D_V and, as a rule, $\Delta = 10^3$–10^5 [116]. The diffusion coefficient along the grain boundaries (D_{Gb}), which includes diffusion parallel to grain boundaries (D_b) and surface diffusion (D_S), is not a characteristic of the material, but depends on the properties of the boundary, *i.e.* its structure. For low-angle grain boundaries (misorientation <15°), D_{Gb} differs weakly from D_V. The value of

D_{Gb} (at a given axis of rotation) increases with increasing angle of rotation. For some boundaries with a highly ordered (bulk [50–52] or planar [117–120]) structure and close-packed grains, extremely low diffusion coefficients D_{Gb} are observed. For a direction, parallel to the dislocation lines, *i.e.* parallel to the axis of rotation, diffusion is faster than in the perpendicular direction, where diffusion, as a rule, is a bulk. Such anisotropy is confirmed experimentally. With an increase in the angle of rotation, the anisotropy decreases, but with a misorientation of more than 15°, a significant anisotropy of the diffusion coefficient conserves. Comparison of the bulk, parallel to grain boundaries, and surface diffusion, showed that the smallest activation energy is observed for the surface diffusion, while the greatest one for bulk diffusion. If assume that the pre-exponential coefficient D_0 has approximately the same value independently on the diffusion type, then in accordance with the Arrhenius dependence the highest diffusion coefficient is observed for the surface diffusion, and the lowest for the bulk diffusion [85].

At the same temperature, not all atoms have the same mobility. Atoms located on the surface of the particles and, especially on their protrusions (humps), have greater mobility. Therefore, surface atoms (especially those located at the humps) possess the greatest displacements in the initial sintering stage. Such atoms possess the greatest surface energy and can easily leave their places, trying to occupy more stable positions in the valleys (hollows, cavities) of the particles. Highly mobile atoms are concentrated in narrow areas of the interparticle space and begin to belong simultaneously to several particles. Such surface diffusion leads to an increase in interparticle contacts and to the hardening of powder solids. The most effective manifestation of surface diffusion is observed at low and medium sintering temperatures.

At high temperatures, a significant role belongs to the bulk diffusion, which results to decrease of the mechanical strength of particles, increase of plasticity, and their ability to flow in a metal under the action of surface tension forces [121]. With an increase of the annealing time, the grain-boundary peaks in the concentration distribution graph are gradually smoothed and, as a result, it is becoming more difficult to observe experimentally accelerated diffusion along the grain boundaries. The optimal conditions for determining the parameters of grain boundary diffusion are that the value β has to be at least more than 10, in order to determine accurately coefficient of the grain boundary diffusion D_b from the experiments on different layers. The duration of diffusion annealing should be chosen in accordance with this requirement [37].

In the work [114], there is no expression for an average diffusant concentration $\bar{c}$; therefore, the solution in Ref. [115] will be further used. This solution is obtained for diffusion from an instant source —

diffusion from a thin-film source on the sample surface with a very small film thickness δ.

The equation for the concentration of diffusant in the grain $c_g(y, z, \tau)$ reads in a short form as

$$c_g(\varepsilon, \eta, \beta) = c_1(\eta) + c_2(\varepsilon, \eta, \beta), \tag{43}$$

where c_1 is the contribution of direct bulk diffusion from a source with a constant concentration to the bulk in the z-direction, and c_2 is the contribution of the grain boundary.

The exact solution for the diffusion equation from an 'instantaneous' source (or thin-film) was obtained in Ref. [115]. Since c_1 decreases much faster than c_2, then in the area far from the source, $c_1 \ll c_2$. Therefore, almost the entire diffusant located in this region comes there via the bulk diffusion from the grain boundary and, consequently, far from the diffusion source, $\overline{c} = \overline{c}_2$.

The coefficient of grain-boundary diffusion is substantially greater than the bulk diffusion coefficient and, as a rule,

$$\Delta = D_b/D_V. \tag{44}$$

From the second equality in Eq. (42), we have:

$$\beta = \delta D_b/(2D_V^{3/2}\tau^{1/2}) = (\delta/2)(D_b/D_V)(D_V\tau)^{-1/2}. \tag{45}$$

Considering the approximate equality $D_V \cong 10^{-4}D_b$ and Arrhenius formula $D_b = D_{b0}\exp(-E_b/RT)$, where an activation energy of grain boundary diffusion E_b = 200–300 kJ/mole for most metal alloys, we find that even at sufficiently high temperatures T:

$$\beta \gg 10^2. \tag{46}$$

Let us consider two cases: (i) $10^2 < \beta < 10^4$ and (ii) $\beta \gg 10^4$.

In Ref. [37], for these cases, simplified versions of the equations for calculating the product δD_b for an 'instantaneous' source are reported. For the first (i) case:

$$\delta D_b = 0.2968D^{585/119}\tau^{-121/133}(-\partial \lg \overline{c}/\partial z^{6/5})^{-200/119}; \tag{47}$$

for the second (ii) case:

$$\delta D_b = 2(D_V\tau)^{-1/2}(-\partial \lg \overline{c}/\partial z^{6/5})^{-5/3}(0.775)^{5/3}, \tag{48}$$

where $\overline{c}$ is the average concentration of the diffusant, and z is the depth of its penetration into the grain from the instantaneous source (this is how [115] the diffusion from the thin-film source on the sample surface with a very small film thickness δ is of the order of the atomic diameter). Using the advantage of the approach in Ref. [116], there is the following relation for a source of finite thickness:

$$-\partial \lg \overline{c}/\partial z^{6/5} = 0.314\beta^{-0.592}. \tag{49}$$

Substituting the expression from (42) into Eq. (47) and assuming $0.9849 \approx 1$, we obtain for the first (i) case:

$$\delta D_b = 0.2968 D_V^{4.916} \tau^{0.5084} (0.314)^{-1.68} \delta D_b / (2 D_V^{1.5} \tau^{0.5}), \quad (50)$$

where one can find out

$$D_V = 0.9932 \tau^{0.295}. \quad (51)$$

Since $D_b/D_V = \Delta$, Eq. (50) can be written as

$$D_b = 0.1484 D_V^{4.416} \tau^{-1.0084} (0.314)^{-1.68} \Delta, \quad (52)$$

from which, taking into account Eq. (51) for D_V, we obtain

$$D_b = 1.0090 \Delta \tau^{0.295}. \quad (53)$$

In the second (ii) case, Eqs. (48) and (49) result to

$$\delta D_b = 0.32587 D_V^{0.5} \tau^{-0.5} (0.314)^{-1.67} \beta^{0.9866}. \quad (54)$$

Substituting β from Eq. (42) and assuming $0.9866 \approx 1$, we obtain

$$\delta D_b = 0.32587 D_V^{0.5} \tau^{-0.5} (0.314)^{-1.67} (\delta D_b / 2 D_V^{1/5} \tau^{0.5}), \quad (55)$$

and

$$D_V = 1.1262 \tau^{-1}. \quad (56)$$

Eq. (54) can be written in the form

$$\delta D_b = 0.32587 D_V^{0.5} \tau^{-0.5} (0.314)^{-1.67} (\delta/2)(\Delta/(2 D_V^{0/5} \tau^{0.5})), \quad (57)$$

which results to

$$D_b = 1.1262 \tau^{-1}. \quad (58)$$

Relations (50) and (53) as well as (56) and (58) have a physical meaning, if the dependence of τ on T is known. We use formulas (51) and (53) for numerical integration of the Eqs. (15)–(19):

$$D_{V,ij} = 0.9932 \tau_{ij}^{0.295}, \; D_{b,ij} = 1.0089 \tau_{ij}^{0.295}, \quad (59)$$

where

$$\tau_b = h_i^j = t_{i,j} - t_{i-1,j} = (T_{i,j} - T_{i-1,j})/w_{T_j}.$$

Sintering of multicomponent systems is characterized by a series of features consisting in the fact that sintering of dissimilar materials is a more complex eutectic process, in which, along with self-diffusion, causing mass transfer to the particle contact area, an interdiffusion (heterodiffusion) should occur, providing balancing of the concentrations of opposite atoms within the sample. With limited solubility or complete insolubility of the components, the sintering system is complicated by isolating homogeneous particles from mutual contact, which prevents self-diffusion from occurring and worsens sintering conditions.

We study mixture of powders consisting of iron (44%), grey cast iron (50%), and 6% of sitallized glass (sitall). Iron compound with sitall (Fe_2SiO_4 — fayalite) will be considered as component A, and iron compound with carbon (cast iron) — component B. The heterodiffusion coefficient D of the binary system of components A and B is expressed in terms of the partial diffusion coefficients [23]:

$$\tilde{D} = c_B D_A + c_A D_B; \quad (60)$$

we consider the case when concentrations of the components A and B are equal, $c_A = c_B = 0.5$. Darken's theory has been criticized many times; however, it is in quite good agreement with experiments [23].

The diffusion coefficient determined in experiments is a certain average value of the diffusion coefficient along the grain boundaries D_{Gb} (including D_b and D_S) and the bulk diffusion coefficient [116]:

$$\tilde{D} = (D_b + D_V + D_S)/3. \quad (61)$$

The coefficient D_A is defined in Eq. (40); D_B is contained in Table 2. Knowing D_b, D_V and $\tilde{D}$, we can calculate D_S using Eq. (61).

2.6. Simulation Approach for Sintering of Powder Mixture

Constructing a model of the powder sintering process, we accept assumptions [71] following below.

- material grains are single crystal and the average grain size is taken as the structural parameter of the material;
- compaction of the material at the stage of sintering in vacuum is carried out by the mechanism of diffusion-viscous flow with thermal slipping along the grain boundaries and decreasing the volume of pores due to the pushing of voids onto the surface;
- the growth of material grains occurs due to thermally activated diffusion coalescence of dispersed particles with the redistribution of the small particles along the surface of larger particles under the action of surface self-diffusion, localized in the surface (one atomic diameter δ thick) layer;
- in the rheological description of the porous structure, the Mackenzie–Shuttleworth model [61] is used, in accordance with which the phase of void is localized in an ensemble of interacting equal spherical pores displaced with respect to each other so far that the porous material can be represented as a set of elements, each of which includes a pore surrounded by a layer of incompressible matter;
- compaction at the stage of sintering under pressure (acting on the solid as a comprehensive compression) is carried out according to the mechanism of viscous flow;
- temperature (T_j, $j = 1, \ldots, n$) does not vary over the volume of the sintering space with a temperature equal to the temperature of the material.

Let us define $\Delta_{1j} = (t_{j-1}, t_j)$ ($j = 1, \ldots, n$) as the time intervals of non-isothermal sintering with temperature T_j supported on the interval Δ_{1j} of duration τ_{1j}, where $t_j = \Sigma_{l=1}^{j}\tau_{1j}$. Define $\Delta_2 = (t_n, t_n + \tau_2)$ as the time interval of isothermal sintering with duration τ_2 with the constant temperature T_C. Denote the average sizes of grains and porosity in the interval Δ_{1j} ($j = 1, \ldots, n$) or Δ_2 as Π_{1j} and L_{1j} or Π_2 and L_2, respectively.

To describe a stage of the solid phase sintering, we use a model including mathematical equations and conditions following below.

• Equation of the kinetics of compaction of the material at the j-th temperature stage (see also Eqs. (20), (20′) and (20″)):

$$\frac{d\Pi_{1,j}}{dt} = -\frac{6(1-\Pi_{1,j})^{3/2}\cdot 3^{2.1}}{(1-\Pi_0)^{1/2}\left[1-\left((1-\Pi_0)/(1-\Pi_{1,j})\right)^{1/2}\right]^{2.1}}\times$$

$$\times\left\{\frac{2\gamma\Omega D_{V,j}}{3k_BT_jr_g^3}\left[1-\left(\frac{1-\Pi_0}{1-\Pi_{1,j}}\right)^{1/2}\right]+\frac{\gamma\Omega bD_{b,j}}{2k_BT_{1,j}r_g^4}\right\}; \tag{62}$$

for the first 3.5% of shrinkage, the kinetic equation reads as

$$\frac{d\Pi_{1,j}}{dt} = -\frac{6(1-\Pi_{1,j})^{3/2}\cdot 3^{2.06}}{(1-\Pi_0)^{1/2}\left[1-\left((1-\Pi_0)/(1-\Pi_{1,j})\right)^{1/2}\right]^{2.06}}\times$$

$$\times\left\{\frac{2.63\gamma\Omega D_{V,j}}{3^{1.03}k_BT_jr_g^3}\left[1-\left(\frac{1-\Pi_0}{1-\Pi_{1,j}}\right)^{1/2}\right]^{1.03}+\frac{0.7\gamma\Omega bD_{b,j}}{2k_BT_{1,j}r_g^4}\right\}, \tag{62′}$$

where $D_{b,j}$ and $D_{V,j}$ are the coefficients of grain-boundary and bulk diffusion (m^2/s), k_B is the Boltzmann constant in units of J/K, T_j is the temperature at the j-stage of sintering (K), Π_0 is the porosity before the start of sintering, Π_{1j} porosity at the j-stage of sintering.

• Equation of the kinetics of grain growth (see also Eq. (22)):

$$dL_{1,j}/dt = B_1\gamma D_{S,j}\delta^4/(4L_{1,j}^3kT_j); \tag{63}$$

here $D_{S,j}$ is the surface diffusion coefficient, $L_{1,j} - L_0$ is the thickness of the layer (of the order of the atomic diameter δ) in which surface diffusion takes place, γ is the surface tension, T_j is the absolute temperature at the j-stage of sintering, numerical constant $B_1 \approx 30$.

• Equation of temperature rise:

$$dT_j/dt = w_{T_j},\ w_{T_j} = (T_j - T_{j-1})/\tau_{1j},\ t_{j-1} < t \le t_j. \tag{64}$$

• Initial conditions:

$$\Pi\big|_{t=0} = \Pi_0,\ L\big|_{t=0} = L_0,\ T\big|_{t=0} = T_0. \tag{65}$$

• Conditions of conjugation of temperature stages in time:

$$\Pi_{1,j}\big|_{t=t_{j-1}} = \Pi_{1,j-1},\ L_{1,j}\big|_{t=t_{j-1}} = L_{1,j-1},\ T\big|_{t=t_{j-1}} = T_{j-1},\ j = 2,\ \ldots,\ n. \tag{66}$$

The conjugation conditions (66) at the junctions of the temperature stages carry out the continuous join of solution obtained for the individual temperature stages. The values obtained in this way for porosity Π_t and graininess L_t at $t = t_n$ will be used as initial data for liquid-phase sintering.

Note that at low and medium annealing temperatures, $D_b \gg D_V$. In this case, we can use the kinetic equation (19) applicable if the grain-boundary diffusion dominates over the bulk diffusion. Taking into account relation between $d\Pi_c/dt$ and dy/dt, we obtain the following equation for the kinetics of compaction at the j-th temperature regime (stage):

$$\frac{d\Pi_{1,j}}{dt} = \frac{-6(1-\Pi_{1,j})^{1.5}}{(1-\Pi_0)^{0.5}} \cdot 0,33 \left(\frac{2.14\gamma\Omega b D_{b,j}}{k_B T_{1,j} r_g^4} \right)^{0.33} t^{-0.67},$$

which can be used for all $t \in \Delta_{1j}$ starting with $j = 2$ to $j = n$.

The main difference between liquid-phase sintering and solid-phase sintering is that (along with a change of capillary forces in the contact of particles) when a melt (wetting the particles) appears, the surface area of interacting components increases significantly. This circumstance strongly accelerates the process of alloy formation, and the thermal and bulk effects (associated with it) become apparent immediately [46]. At once of the contact with the solid phase, liquid phase atoms begin to diffuse into the solid surface. Such diffusion in the first stage of interaction between the solid and liquid phases causes an increase in the volume of the particles of the component (which is the basis of the powder solid) and the separation of the particle centres (which leads to an increase in the linear dimensions of the entire melt). The subsequent dissolution of particles of the solid phase in the liquid is accompanied by a decrease of their volume, the approaching of their geometric centres due to the impact of capillary forces and, as a result, an increase of the shrinkage of the powder solid. Thus, after the formation of a liquid phase during sintering of a powder solid, in a general case, firstly, the growth emerges, and then it is followed by the shrinkage (compaction) [47].

The kinetics of compaction at the stage of liquid-phase sintering will be analysed based on the rheological description of the deformation of the porous structure considering diffusion-viscous flow and compaction of the porous solid under the uniform stressed state in conditions of the uniform compression [24].

Such formulation of the problem characterizes the sintering process with simultaneous effects of both Laplace (capillary) pressure P_c and hydrostatic pressure P applied externally and obtained by summation of the capillary pressure P_c with the inert gas pressure on the material P_g: $P = P_c + P_k$.

Following the hydrodynamic analogy of the theory of elasticity, it can be assumed that in an isotropic medium, the viscosity tensor has two components: the bulk (χ) and shear (η) viscosity coefficients. They are similar to those used in the mechanics: compression (K) and shear (G) moduli. However, in contrast to a non-porous solid, in which there are no internal degrees of freedom for the mutual change of its parts

and the modules K and G are large, in a porous solid, where there is such a freedom, the values of χ and η coefficients are significantly smaller and depend on porosity.

To describe the dimensionless bulk deformation under the uniform compression, one can use the relation [47]:

$$\Delta V/V = \varepsilon_{ii} = -P/\chi, \tag{67}$$

where ε_{ii} is the sum of the diagonal terms of the strain tensor.

Based on the hydrodynamic analogy of the theory of elasticity, since the state-of-the-art version of the rheological sintering theory [59] is based on this analogy, we can write the following viscous flow equation for a compressible solid [24]:

$$\dot{V}/V = \dot{\varepsilon}_{ii} = 3\dot{\varepsilon}_{rr} = -P/\chi; \tag{68}$$

since, in the above formulation of the problem, the strain rate tensor is spherically symmetric and can be reduced to one radial component $\dot{\varepsilon}_{rr}$. Taking into account the obvious relation between the volume of the porous solid, V, and the volume of the matter contained in it (without pores), V_B, $V = V_B(1 - \Pi)$, we obtain

$$\dot{V}/V = \dot{\Pi}(1 - \Pi); \tag{69}$$

here Π is a dimensionless porosity of the solid.

In the rheological description of the porous structure (χ, η), the Mackenzie–Shuttleworth model is accepted, according to which the phase of void can be represented as localized in an ensemble of non-interacting equal-size pores, which are distant from each other. Moreover, they are distant do far that one can introduce into consideration an element of a porous solid consisting of a pore radius R surrounded by a layer of an incompressible solid with radius R° with $\Pi = (R/R^{\circ})^3$.

From the hydrodynamic analogy, the relationship between χ and η is given by the relation

$$\chi = 4\eta(1 - \Pi)/3\Pi. \tag{70}$$

From relations (68) and (69), we obtain the following law of compaction of a porous solid:

$$d\Pi/dt = -(1 - \Pi)P/\chi \tag{71}$$

or using Eq. (70)

$$d\Pi/dt = -3\Pi P/(4\eta). \tag{72}$$

Taking into account the dependence of the coefficient of shear viscosity of a porous solid η on porosity Π established in Refs. [59–61],

$$\eta = \eta_0(1 - \Pi)^{5/3}, \tag{73}$$

the differential equation of a porous solid (72) can be written as

$$d\Pi/dt = -3\Pi P/[4(1 - \Pi)^{5/3}\eta_0]. \tag{74}$$

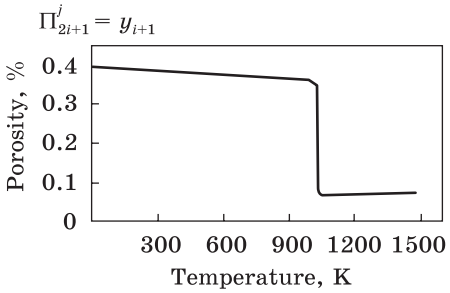

Fig. 3. Temperature dependence of porosity

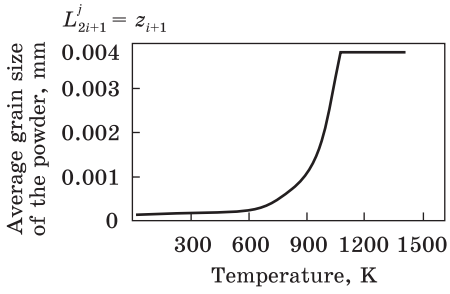

Fig. 4. Temperature-dependent average grain size of the powder

For small porosities, we can restrict ourselves to the linear dependence of η on Π, assuming $(1 - \Pi)^{5/3} \simeq 1 - (5/3)\Pi$. Then, we obtain the following law of compaction of a porous solid [59]:

$$d\Pi/dt = -(3/4)[\Pi/(1 - 5\Pi/3)](P/\eta_0). \quad (75)$$

Equations for the mathematical description of the stage of isothermal (liquid phase) sintering under pressure P includes:

equation of the kinetics of compaction of the material (see Eq. (74)):

$$d\Pi_2/dt = -[\Pi_2/(1 - \Pi_2)^{5/3}]3P/(4\eta_0),\ t \in \Delta_2; \quad (76)$$

rheological model of porous material (see equations (70), (73)):

$$\chi = 4\eta(1 - \Pi_2)/3\Pi_2,\ \eta = \eta_0(1 - \Pi_2)^{5/3}; \quad (77)$$

equation of grain growth kinetics of the material:

$$dL_2/dt = B_1\gamma D_{s,n}\delta^4/(4L_2^3kT_c),\ t \in \Delta_2, \quad (78)$$

where $D_{s,n}$ relates with activation energy of the grain-boundary diffusion (Q_s),

$$D_{s,n} = D_{s,0}\exp(-Q_s/RT_c). \quad (79)$$

The capillary pressure P_c applied to the pore surface and the instantaneous radius of pore R_p are determined by the equations [71]

$$P_c = 2\Pi_2\sigma/R_p,\ P_p = R_{p^\circ}(1 - \Pi_{1,n})/[\Pi_{1,n}(1 - \Pi_2)], \quad (80)$$

where $\sigma = 2\pi/R_{p^\circ}$ is the surface pressure, R_{p° is the radius of the grains before sintering; initial conditions read as

$$\Pi_2\big|_{t=t_n} = \Pi_{1,j}\big|_{t=t_n},\ L_2\big|_{t=t_n} = L_{1,j}(t)\big|_{t=t_n},\ T_c = T_n. \quad (81)$$

The density of the material at the stages of the process is calculated depending on its current porosity using the equations:

$$\rho_{1,j} = (1 - \Pi_{1,j}(t))\rho_0,\ (j = 1, \ldots, n),\ \rho_2 = (1 - \Pi_2(t))\rho_v. \quad (82)$$

Volumetric shrinkage of the stages is calculated by the equations:

$$\Delta V_{1,j}/V_0 = (V_0 - m/\rho_{1,j})/V_0,\ (j = 1, ..., n),\ \Delta V_2/V_0 = (V_0 - m/\rho_2)/V_0, \quad (83)$$

where $\Delta V_{1,j} = V_0 - V_{1,j}$, $\Delta V_2 = V_0 - V_2$, and m is mass of the sample.

The quality index (residual porosity Π_p, average grain size L_p, and density ρ_p) of the alloy can be determined from the relations:

$$\Pi_p = \Pi_2(\tau_1 + \tau_2),\ L_p = L_2(\tau_1 + \tau_2),\ \rho_p = \rho_2/(\tau_1 + \tau_2).$$

If we know D, D_V, and D_b, one can determine D_s as a function of T and τ, which gives a possibility to calculate (*via* the fourth order Runge–Kutta method) porosity Π and graininess in discrete points t_{ij} ($i = 1, ..., M_1$; $j = 1, ..., n$) over all time interval of the solid-phase sintering. Representative results in Fig. 3, Fig. 4 are plotted for $10^2 < \beta < 10^4$ and $\Delta = 10^2$.

3. Summary

For the mathematical description of the process of sintering a mixture of powders, a system of nonlinear differential equations of the kinetics of compaction and grain growth for sequential temperature regimes is constructed. By fitting the solutions of these equations at the junctions of temperature regimes and integrating the resulting system of equations using the fourth order Runge–Kutta method, the numerical time discretization of continuous porosity and grain curves is constructed.

The investigated mixture of iron powders, grey cast iron, and sitallized glass (sitall) is considered as a system of two components. A compound of iron with a sitall (fayalite) represents the first component; the second component is a compound of iron with carbon (cast iron). The Darken formula is applied to calculate the interdiffusion coefficient of this (quasi)binary system.

In the rheological description of the sintering kinetics under pressure (uniform compression), the mechanism of diffusion-viscous flow was used within the framework of the Mackenzie–Shuttleworth model. In accordance with this mechanism, thermal slippage occurs along the grain boundaries and a decrease of the pore volume due to the ejection of vacancies on the surface.

During the process of formation of a liquid phase, the capillary forces at the contact of the particles vary. When a melt (wetting the particles) appears, the surface area of interaction between the components increases significantly that accelerates the sintering process. At the same time, in the process of sintering a powder solid, one can observe a decrease of porosity and an increase of graininess. Then, the shrinkage and stabilization of both porosity and graininess occurs.

The proposed algorithm for numerical simulation of compaction kinetics for solid-phase sintering of highly dispersed and, particularly,

nanosize powders allows analysing and controlling the technical parameters of the process of solid-phase sintering of metal-ceramic alloys. The calculated values of these parameters (obtained as a result of solid phase sintering, are used as their input values in the process of liquid-phase sintering [122].

REFERENCES

1. O.I. Raichenko, *Metallofiz. Noveishie Tekhnol.*, **38**, No. 5: 635 (2016) (in Russian). https://doi.org/10.15407/mfint.38.05.0635
2. A. Boudilmi and K. Loucif, *Metallofiz. Noveishie Tekhnol.*, **40**, No. 12: 1689 (2018). https://doi.org/10.15407/mfint.40.12.1689
3. D.S. Kanibolotsky, O.A. Shcheretskyi, M.V. Afanasiev, and A.M. Verkhovliuk, *Metallofiz. Noveishie Tekhnol.*, **39**, No. 11: 1481 (2017) (in Russian). https://doi.org/10.15407/mfint.39.11.1481
4. V.V. Gunina, V.G. Mel'nikov, and N.I. Zamyatina, *Fizika, Khimiya i Mekhanika Tribosistem: Mezhvuzovskiy Sbornik Nauchnykh Trudov* (Ivanovo: Ivanovo State University: 2002), p. 96 (in Russian).
5. M.V. Kirsanov, *Metalosteklyannyye Kompozitsionnyye Materialy na Osnove Vysokomargantsevistoy Stali 110Г13Л* [Metal-Glass Composite Materials Based on 110Г13Л High-Manganese Steel] (Disser. for Cand. Tech. Sci.) (Novocherkassk: South-Russian State Tech. Univ.: 2000) (in Russian).
6. D. Brigante, *New Compozite Materials: Selection, Design and Application* (Switzerland: Springer International Publishing: 2014). https://doi.org/10.1007/978-3-319-01637-5
7. R.M. German, *Particulate Composites: Fundamentals and Applications* (Switzerland: Springer International Publishing: 2016). https://doi.org/0.1007/978-3-319-29917-4
8. D.A. Oshchenkov, *Tekhnologiya, Struktura i Svoistva Tribotekhnicheskikh Materialov na Osnove Poroshkov Nerzhaveyushchikh Staley* [Technology, Structure and Properties Tribotechnical Materials Based on Powder Stainless Steels] (Disser. for Cand. Tech. Sci.) (Perm: Perm State Techn. Univ.: 2006) (in Russian).
9. J. Tengzelius and A.B. Нцандз, *PM Asia 2007 (April, 2007, Shanghai)*.
10. V.V. Gunina, *Prochnostnyye i Antifriktsionnyye Svoistva Poroshkovogo Bronzografita s Napolnitelyami* (Depon. VINITI: 14.03.2005), 340-И (in Russian).
11. A.H. Monazzah, H. Powaliakbar, R. Baghu, and S.M.S. Reihani, *Composites Part B: Eng.*, **125**: 49 (2017). https://doi.org/10.1016/j.compositesb.2017.05.055
12. S.V. Bobyr, *Metallofiz. Noveishie Tekhnol.*, **40**, No. 11: 1437 (2018) (in Russian). https://doi.org/10.15407/mfint.40.11.1437
13. H.I. Imanov, I.D. Sadyhov, A.T. Mamedov, and T.G. Jabbarov, *Sci. and Tech. Conf. 'Novyye Materialy v Povyshenii Ehkspluatatsionnoi Nadezhnosti Mashin i Instrumentov — AzITU* (Baku, 1990), p. 47.
14. T.G. Jabbarov, *Razrabotka Kompozitsionnykh Poroshkovykh Materialov 'Zhelezo–Chugun–Steklo' dlya Detalei Bytovoi Tekhniki* [Development of Composite Powder Materials 'Iron–Cast Iron–Glass' for Household Appliance Components] (Disser. for Cand. Tech. Sci.) (Novocherkassk: 1992) (in Russian).
15. G.A. Libenson, V.Yu. Lopatin, and G.V. Komarnackiy, *Protsessy Poroshkovoy Metallurgii* [Processes of Powder Metallurgy] (Moscow: MISIS: 2002), Vol. 2 (in Russian).

16. O.V. Roman, *Poroshkovyye Stali* [Powder Steels] (Moscow: Mashinostroenie: 2000), Vol. 2 (in Russian).
17. A.B. Höganäs, *Höganäs Handbook for Sintered Compaction* (Sweden: 2004).
18. B.Ya. Pines, *ZhTF*, **16**: 137 (1946).
19. G.C. Kyszynski, *J. Appl. Phys.*, **20**: 1160 (1949). https://doi.org/10.1063/1.1698291
20. 20. C. Herring, *The Physics of Powder Metallurgy* (Ed. W. E. Kingston) (New York.: Mc Graw Hill: 1951).
21. Ya.E. Geguzin and V.I. Kudrik, *Fiz. Met. Metalloved.*, **7**: 235 (1959) (in Russian).
22. I.M. Lifshitz and V.V. Slezov, *ZhETF*, **35**: 479 (1958) (in Russian).
23. *Protsessy Vzaimnoj Diffuzii v Splavakh* [Processes of Interdiffusion in Alloys] (Ed. K.P. Gurov) (Moscow: Nauka, Fizmatlit: 1973) (in Russian).
24. Ya.E. Geguzin, *Fizika Spekaniya* [Physics of Sintering] (Moscow: Nauka, Fizmat: 1984) (in Russian).
25. V.A. Ivensen, *Fenomenologiya Spekaniya i Nekotoryye Voprosy Teorii* [Phenomenology of Sintering and Some Problems of Theory] (Moscow: Metallurgiya: 1985) (in Russian).
26. V.N. Antsiferov, S.N. Peshcherenko, and P.G. Kurilov, *Vzaimnaya Diffuziya i Gomogenizatsiya v Poroshkovykh Materialakh* [Interdiffusion and Homogenization of Powder Materials] (Moscow: Metallurgiya: 1988) (in Russian).
27. Yu.M. Mishin and I.M. Razumovskiy, *Struktura i Svoistva Vnutrennikh Poverhnostey Razdela v Metallakh* [Structure and Properties of Internal Interfaces in Metals] (Moscow: Nauka: 1988), p. 96 (in Russian).
28. V.V. Skorohod, Yu.M. Solonin, and I.V. Uvarova, *Khimicheskie, Diffuzionnyye i Reologicheskie Protsessy v Tekhnologii Poroshkovykh Materialov* [Chemical, Diffusion and Rheological Processes in the Powder Materials Technology] (Kiev: Naukova Dumka: 1990) (in Russian).
29. Yu.R. Kolobov, *Diffuzionno-Kontroliruemyye Protsessy na Granitsakh Zeren i Plastichnost Metallicheskikh Polikristallov* [Diffusion-Controlled Processes on the Grain Boundaries and Plasticity of Metallic Polycrystals] (Moscow: Nauka, Sibirskoe Predpriyatie RAN: 1998) (in Russian).
30. Yu.R. Kolobov, A.G. Lipnitsky, M.B. Ivanov, and E.V. Golosov, *Composites and Nanostructures*, No. 2: 5 (2009) (in Russian).
31. A.V. Ragulya, *Nauchnyye Osnovy Upravlyayemykh Neizotermicheskikh Protsessov Sinteza i Spekaniya Nanostrukturnykh Materialov* [Scientidic Bases of Controllable Nonisothermic Processes of Synthesis and Sintering Nanostructural Materials] (Disser. for Dr. Tech, Sci.) (Kiev: I. N. Frantsevich Inst. for Problems of Mater. Sci.: 2001) (in Russian).
32. A.V. Ragulya and V.V. Skorohod, *Konsolidirovannyye Nanostrukturnyye Materialy* [Consolidated Nanostructural Materials] (Kiev: Naukova Dumka: 2007) (in Russian).
33. D.L. Johnson, *J. Appl. Phys.*, **40**, No. 1: 192 (1969). https://doi.org/10.1063/1.1657030
34. T.E. Volin, K.H. Lie, and R.W. Balluffi, *Acta Met.*, **19**, No. 4: 263 (1971). https://doi.org/10.1016/0001-6160(71)90092-7
35. H.E. Exner, *Principles of Single Phase Sintering* (Tel-Aviv: Freund Publishing House: 1979), Vol. **1**, Nos. 1/4, Series *Reviews on powder metallurgy and physical ceramics*.
36. I. Kaur, Yu. Mishin, and W. Gust, *Fundamentals of Grain and Interphase Boundary Diffusion* (West Sussex: John Willey and Sons LTD: 1995).

37. I. Kaur and V. Gust, *Diffuziya po Granitsam Zeren i Faz* [Diffusion over Grain Boundaries and Phases] (Moscow: Mashinostroenie: 1991) (in Russian).
38. G.P. Cherepanov, *Methods of Fracture Mechanics: Solid Matter Physics. Solid Mechanics and Its Applications* (Dordrecht: Springer: 1997), Vol. **51**, p. 84. https://doi.org/10.1007/978-94-017-2262-9_4
39. A.M. Gusak and G.V. Lutsenko, *Powder Metall. Met. Ceram.*, **38**: 569 (1999). https://doi.org/10.1007/BF02676188
40. Yu.N. Ivashchenko, B.B. Bogatyrenko, and V.N. Eremenko, *Poverkhnostnyye Yavleniya v Rasplavakh i Protsessakh Poroshkovoy Metallurgii* (Kiev: Izdatelstvo AN USSR: 1963), p. 391 (in Russian).
41. G.H.S. Price, C.J. Smithells, and S.V. Williams, *J. Inst. Metals*, **62**: 239 (1938).
42. H.S. Cannon and F.V. Lenel, *Proc. First Plansee Seminar* (Ed. F. Benesovsley) (Reutte, Austria, 1953), p. 106.
43. W.D. Kingery, *J. Appl. Phys.*, **30**, No. 3: 301 (1959). https://doi.org/10.1063/1.1735155
44. V.N. Eremenko, *Poverkhnostnyye Yavleniya v Rasplavakh i Protsessakh Poroshkovoy Metallurgii* (Kiev: Izdatelstvo AN USSR: 1963), p. 83 (in Russian).
45. I.P. Kislyakov, *Uplotnenie, Poverkhnostnyye Yavleniya v Rasplavakh i Protsessakh Poroshkovoy Metallurgii* (Kiev: Izdatelstvo AN USSR: 1963), p. 182 (in Russian).
46. V.V. Skorokhod, S.M. Solonin, V.A. Dubok, L.L. Kolomiets, T.V. Permyakova, and A.V. Shinkaruk, *Powder Metall. Met. Ceram.*, **49**, Nos. 9–11: 588 (2011). https://doi.org/10.1007/s11106-011-9274-4
47. A.P. Savitskiy, *Zhidkofaznoye Spekanie Sistem s Vzaimodeistvuyushchimi Komponentami* (Novosibirsk: Nauka, Sibirskoe Otdelenie: 1991), p. 184.
48. T.M. Radchenko and V.A. Tatarenko, *Defect Diffus. Forum*, **273–276**: 525 (2008). https://doi.org/10.4028/www.scientific.net/DDF.273-276.525
49. T.M. Radchenko, V.A. Tatarenko, and S.M. Bokoch, *Metallofiz. Noveishie Tekhnol.*, **28**, No. 12: 1699 (2006).
50. A.G. Khachaturyan, *Prog. Mater. Sci.*, **22**, Nos. 1–2: 1 (1978). https://doi.org/10.1016/0079-6425(78)90003-8
51. T.M. Radchenko, V.A. Tatarenko, H. Zapolsky, and D. Blavette, *J. Alloys and Compounds*, **452**, No. 1: 122 (2008). https://doi.org/10.1016/j.jallcom.2006.12.149
52. T.M. Radchenko, V.A. Tatarenko, and H. Zapolsky, *Solid State Phenomena*, **138**: 283 (2008). https://doi.org/10.4028/www.scientific.net/SSP.138.283
53. V.S. Panov, *Russ. J. Non-Ferrous Metals*, **48**, No. 2: 148 (2007) (in Russian). https://doi.org/10.3103/S1067821207020149
54. Yu.R. Kolobov, V.A. Vinokurov, E.V. Naidenkin et al. *Sposob Polucheniya Materialov s Ul'tramelkozernistoy ili Sublikristallicheskoy Strukturoy Defor mirovaniem s Obestocheniem Intensivnoy Plasticheskoy Deformatsii* (Patent RF T2334582.13.07.2008) (in Russian).
55. V.N. Antsiferov and I.V. Anciferova, *Vestnik Permskogo Natsional'nogo Issledovatel'skogo Politekhnicheskogo Universiteta. Mashinostroenie, Materialovedenie*, **17**, No. 2: 66 (2015) (in Russian).
56. I.V. Anciferova, *Vestnik Permskogo Natsional'nogo Issledovatel'skogo Politekhnicheskogo Universiteta. Mashinostroenie, Materialovedenie*, **17**, No. 2: 13 (2015) (in Russian).
57. L.I. Leont'ev and M.I. Alymov, *Izvestiya Vuzov. Chernaya Metallurgiya*, **59**, No. 5: 306 (2016) (in Russian). https://doi.org/10.17073/0368-0797-2016-5-306-313

58. L.D. Landau and E.M. Lifshitz, *Theory of Elasticity* (Oxford: Elsevier: 1986). https://doi.org/10.1016/C2009-0-25521-8
59. V.V. Skorohod, *Reologicheskie Osnovy Teorii Spekaniya* (Kiev: Naukova Dumka: 1976) (in Russian).
60. J.K. Mackenzie, *Proc. Roy. Soc. B*, **63**, No. 1: 2 (1950). https://doi.org/10.1088/0370-1301/63/1/302
61. J.K. Mackenzie and R. Shuttleworth, *Proc. Phys. Soc. B*, **62**, No. 12: 833 (1949). https://doi.org/10.1088/0370-1301/62/12/310
62. A.I. Berezhnoi, *Glass-Ceramics and Photo-Sitalls* (Boston, MA: Springer: 1970), p. 125. https://doi.org/10.1007/978-1-4684-1761-6_4
63. M.L. Lobanov, I.K. Denisova, and T.M. Rusakov, *Rashchet Kontsentratsionnoy Zavisimosti Koeffitsienta Vzaimnoy Diffuzii v Tverdykh Rastvorakh Dvukhkomponentnykh Sistem* (Ekaterinburg: Ural State Tech. Univ.: 2006) (in Russian).
64. M.L. Lobanov and M.A. Zorina, *Metody Opredeleniya Koeffitsientov Diffuzii: Uchebnoye Posobie* [Methods for Determination of Diffusion Coefficients: Tutorial] (Ekaterinburg: Izdatel'stvo Ural'skogo Universiteta: 2017) (in Russian).
65. L.P. Khoroshun, *Prikladnaya Mekhanika*, No. 10: 30 (2000).
66. V.M. Gorokhov, E.V. Zvonarev, M.S. Koval'chenko, and G. P. Ustinova, *Powder Metall. Met. Ceram.*, **17**, No. 11: 848 (1978). https://doi.org/10.1007/BF00792451
67. V.N. Kokorin, V.I. Filimonov, and E.M. Bulyzhev, *Nauchnyye Osnovy Tekhnologii Pressovaniya iz Polidispersnykh Metallicheskikh Poroshkov s Plotnoupakovannoy Strukturoy* (Ul'yanovsk: UlGTU: 2010) (in Russian).
68. O.P. Shtempel' and V.A. Frutskiy, *Int. Conf. 'Innovation Technologies in Mechanical Engineering' (October 19–20, 2011)* (Novopolotsk: 2011), p. 230 (in Russian).
69. V.K. Sheleg, A.S. Kovgur, and R.A. Moskalets, *Vestnik of Vitebsk State Technological University*, No. 29: 114 (2015).
70. P. Bross and H.E. Exner, *Acta Met.*, **27**, No. 6: 1013 (1979). https://doi.org/10.1016/0001-6160(79)90189-5
71. I.G. Kornienko, T.B. Chistyakova, S.S. Ordan'yan, D.S. Rybin, and A.D. Polosin, *Vestnik Astrakhan State Technical University*, No. 4: 23 (2014) (in Russian).
72. V.V. Kaverynsky, A.I. Trotsan, and Z.P. Sukhenko, *Metallofiz. Noveishie Tekhnol.*, **39**, No. 8: 1051 (2017) (in Russian). https://doi.org/10.15407/mfint.39.08.1051
73. Yu.M. Mishin and N.M. Razumovskiy, *Poverkhnost'*, No. 7: 5 (1983) (in Russian).
74. V.N. Antsiferov, S.N. Peshcherenko, and P.G. Kurilov, *Vzaimnaya Diffuziya i Gomogenizatsiya v Poroshkovykh Materialakh* (Moscow: Metallurgiya: 1988) (in Russian).
75. L.A. Saraev, *Modelirovanie Makroskopicheskikh, Plasticheskikh Svoistv Mnogokomponentnykh Kompozitsionnykh Materialov* (Samara: Izdatel'stvo Samara State Univ.: 2000) (in Russian).
76. A.P. Savitskii, *Tech. Phys.*, **55**, No. 3: 381 (2010). https://doi.org/10.1134/S1063784210030084
77. I.I. Novoselov, A.Yu. Kuksin, and A.V. Yanilkin, *Phys. Solid State*, **56**, No. 7: 1401 (2014). https://doi.org/10.1134/S1063783414070282
78. V.N. Lobko and I.N. Bekman, *Tech. Phys.*, **55**, No. 9: 1306 (2010). https://doi.org/10.1134/S1063784210090124

79. D.L. Johnson and I.B. Cutler, *J. Amer. Ceram. Soc.*, **46**, No. 11: 545 (1963). https://doi.org/10.1111/j.1151-2916.1963.tb14607.x
80. W.D. Kingery and M. Berg, *J. Appl. Phys.*, **26**: 1205 (1955). https://doi.org/10.1063/1.1721874
81. J.G.R. Rocldand, Z. Metalk., **58**: 467 (1967). https://doi.org/10.1111/j.2044-8295.1967.tb01107.x
82. D.L. Johnson and T.M. Clarke, *Acta Met.*, **12**: 1173 (1964). https://doi.org/10.1016/0001-6160(64)90098-7
83. Ya.E. Geguzin, *Makroskopicheskie Defekty v Metallakh* [Macroscopic Defects in Metals] (Moscow: Metallurgiya: 1962) (in Russian).
84. V.V. Skorohod, *Sintering'85* (Eds. G.C. Kuczynski, D.P. Uskoković, H. Palmour, and M.M. Ristić) (Springer: Boston, MA: 1987), p. 81. https://doi.org/10.1007/978-1-4613-2851-3_8
85. Ya.E. Geguzin and Yu.S. Kaganovskij, *Sov. Phys. Usp.*, **21**, No. 7: 611 (1978). https://doi.org/10.1070/PU1978v021n07ABEH005667
86. V.A. Tatarenko, T.M. Radchenko, and V.M. Nadutov, *Metallofiz. Noveishie Tekhnol.*, **25**, No. 10: 1303 (2003) (in Ukrainian).
87. V.A. Tatarenko and T.M. Radchenko, *Intermetallics*, **11**, Nos. 11–12: 1319 (2003). https://doi.org/10.1016/S0966-9795(03)00174-2
88. V.A. Tatarenko, S. M. Bokoch, V.M. Nadutov, T.M. Radchenko, and Y.B. Park, *Defect Diffus. Forum*, **280–281**: 29 (2008). https://doi.org/10.4028/www.scientific.net/DDF.280-281.29
89. G. Gottshtein, *Physical Foundations of Materials Science* (Berlin–Heidelberg: Springer-Verlag: 2004). https://doi.org/10.1007/978-3-662-09291-0
90. H. Mehrer, *Diffusion in Solids* (Berlin–Heidelberg: Springer-Verlag: 2007). https://doi.org/10.1007/978-3-540-71488-0
91. A.G. Stromberg and V.P. Semchenko, *Fizicheskaya Khimiya* (Moscow: Vysshaya Shkola: 2006) (in Russian).
92. V.M. Bezpalchuk, R. Kozubski, and A. M. Gusak, *Uspehi Fiziki Metallov*, **18**, No. 3: 205 (2017). https://doi.org/10.15407/ufm.18.03.205
93. Yu.S. Projdak, V.Z. Kutsova, T.V. Kotova, H.P. Stetsenko, and V.V. Prutchykova, *Uspehi Fiziki Metallov*, **20**, No. 2: 213 (2019). https://doi.org/10.15407/ufm.20.02.213
94. A.I. Berezhnoi, *Glass-Ceramics and Photo-Sitalls* (Boston, MA: Springer: 1970), p. 193. https://doi.org/10.1007/978-1-4684-1761-6_5
95. G.I. Belyaev and N.F. Smakota, *Poverkhnostnyye Yavleniya v Rasplavakh i Protsessakh Poroshkovoy Metallurgii* (Kiev: Naukova Dumka: 1973) (in Russian).
96. Yu.P. Solntsev, E.I. Pryakhin, S.A. Vologzhanina, and A.P. Petkova, *Nanotekhnologii i Spetsial'nyye Materialy* (St. Petersburg: Khimizdat: 2009) (in Russian).
97. R.Z. Vlasyuk, E.S. Lugovskaya I.D. Radomysel'skii, *Powder Metall. Met. Ceram.*, **8**, No. 3: 221 (1980). https://doi.org/10.1007/BF00773577
98. I.D. Radomysel'skiy, *Ehntsiklopediya Neorganicheskikh Materialov* (Kiev: Naukova Dumka: 1977), vol. **1**, p. 808 (in Russian).
99. Y. Zhao, D. Chen, D. Li, J. Peng, and B. Yan, *Metals*, **8**, No. 2: 91 (2018). https://doi.org/10.3390/met8020091
100. M.E. Shaibani, N. Eshraghi, and M. Ghambari, *Mater. Des.*, **47**: 174 (2013). https://doi.org/10.1016/j.matdes.2012.11.058

101. R.J. Borg and G.J. Dienes, *An Introduction to Solid State Diffusion* (Boston: Academic Press: 1988).
https://doi.org/10.1016/C2009-0-22176-3
102. S.K. Sharma, S. Banerjee, Kuldeep, and A. K. Jain, *J. Mater. Res.*, **4**: 603 (1989).
https://doi.org/10.1557/JMR.1989.0603
103. S.K. Sharma, M.-P. Macht, and V. Naundorf, *Acta Metall. Mater.*, **40**: 2439 (1992).
https://doi.org/10.1016/0956-7151(92)90162-8
104. V. Naundorf, M.-P. Macht, A.S. Bakai, and N. Lazarev, *J. Non-Cryst. Solids*, **224**, No. 2: 122 (1998).
https://doi.org/10.1016/S0022-3093(97)00465-1
105. G.B. Fedorov, *Mobility of Atoms in Crystal Lattices* (Ed. V.N. Svechnikov) (Jerusalem: Springfield: 1970), p. 28.
106. M.P. Dariel, *Scr. Metall.*, **8**, No. 7: 869 (1974).
https://doi.org/10.1016/0036-9748(74)90308-1
107. F. Faupel, W. Frank, M.-P. Macht, V. Naundorf, K. Ratzke, H.R. Schober, S.K. Sharma, and H. Teichler, *Rev. Mod. Phys.*, **75**, No. 1: 237 (2003).
https://doi.org/10.1103/RevModPhys.75.237
108. P.G. Shewmon, *Diffusion in Solids* (Cham: Springer Int. Publ.: 2016).
https://doi.org/10.1007/978-3-319-48206-4
109. C. Zener, *Imperfections in Nearly Perfect Crystals* (Eds. W. Shockley, J.H. Holloman, R. Maurer, and F. Seitz) (New York: Wiley: 1952), p. 289.
110. R. Bechmann and R.F.S. Hearmon, *Crystal and Solid State Physics. Elastic, Piezoelectric, Piezooptic and Electrooptic Constants of Crystals* (Eds. K.-H. Hellwege and A. M. Hellwege) (Berlin: Springer: 1966).
111. Y. Limoge and A. Grandjean, *Defect Diffus. Forum*, **143–147**: 747 (1997).
https://doi.org/10.4028/www.scientific.net/DDF.143-147.747
112. S.K. Sharma, M.-P. Macht, and V. Naundorf, *Phys. Rev. B*, **49**: 6655 (1994).
https://doi.org/10.1103/PhysRevB.49.6655
113. J.C. Fisher, *J. Appl. Phys.*, **22**, No. 1: 74 (1951).
https://doi.org/10.1063/1.1699825
114. R.T. Whipple, *Phil. Mag.*, **45**, No. 371: 1225 (1954).
https://doi.org/10.1080/14786441208561131
115. T. Suzuoka, *Trans. Jap. Inst. Metals*, **2**, No. 1: 25 (1961).
https://doi.org/10.2320/matertrans1960.2.25
116. H.S. Levine and Mac Callum, *J. Appl. Phys.*, **31**, No. 3: 595 (1960).
https://doi.org/10.1063/1.1735634
117. T.M. Radchenko, V.A. Tatarenko, I.Yu. Sagalianov, and Yu.I. Prylutskyy, Configurations of Structural Defects in Graphene and Their Effects on Its Transport Properties, *Graphene: Mechanical Properties, Potential Applications and Electrochemical Performance* (Ed. Bruce T. Edwards) (New York: Nova Science Publishers, Inc.: 2014), Ch. 7, p. 219.
118. T.M. Radchenko and V.A. Tatarenko, *Physica E*, **42**, No. 8: 2047 (2010).
https://doi.org/10.1016/j.physe.2010.03.024
119. I.Yu. Sagalyanov, Yu.I. Prylutskyy, T.M. Radchenko, and V.A. Tatarenko, *Uspehi Fiziki Metallov*, **11**, No. 1: 95 (2010).
https://doi.org/10.15407/ufm.11.01.095
120. T.M. Radchenko and V.A. Tatarenko, *Solid State Phenomena*, **150**: 43 (2009).
https://doi.org/10.4028/www.scientific.net/SSP.150.43
121. A.A. Popov and S.V. Grib, *Vzaimnaya Diffuziya v Dvoinykh Sistemakh* (Ekaterinburg: Ural State Tech. Univ.: 2006) (in Russian).

122. R.M. German, P. Suri, and S.J. Park, *J. Mater. Sci.*, **44**, No. 1: 1 (2009). https://doi.org/10.1007/s10853-008-3008-0

Received May 5, 2019;
in final version, October 8, 2019

Т.Г. Джаббаров, О.А. Дишін, М.Б. Бабанли, І.І. Аббасов
Кафедра машинобудування та матеріалознавства,
Азербайджанський державний університет нафти і промисловості,
просп. Азадлиг, 16/21, 1010 Баку, Азербайджан

МАТЕМАТИЧНЕ МОДЕЛЮВАННЯ ПРОЦЕСІВ СПІКАННЯ МЕТАЛОСКЛЯНИХ МАТЕРІАЛІВ НА ОСНОВІ ЗАЛІЗА

На основі дослідження механізмів дифузійної коалесценції та коаґуляції оглядаються математичні методи опису та побудови моделів процесу спікання металокерамічних матеріалів. Ці моделі представлено системою нелінійних диференційних рівнянь, що включають коефіцієнти об'ємної, зерномежової та поверхневої дифузії, а також відповідають послідовності стадійних рівнів температури, зростаючих із певною швидкістю та що мають різні тривалості. Реґулюючи рівні, швидкості та тривалості температурних режимів, технічні параметри шихти, можна контролювати процес спікання в режимі онлайн. Опис кінетики рідкофазового спікання під тиском проведено на основі реологічної теорії спікання з використанням механізму дифузійно-в'язкої течії, відповідно до якого відбувається танґенційне проковзування вздовж меж зерен і зменшення об'єму пор через виштовхування вакансій на поверхню. Після утворення рідкої фази при спіканні порошкового тіла (в загальному випадку) спочатку виявляється зростання зерен, а потім — усадка одержуваного стопу. Процес спікання порошків заліза, чавуну і ситалу розглянуто як взаємну дифузію двох (квази)бінарних стопів: чавуну (залізо + вуглець) і фаяліту (залізо + ситал). Розрахунок коефіцієнта взаємної дифузії результуючого стопу проведено за Даркеновою формулою. Спікання багатокомпонентних систем характеризується рядом особливостей, які полягають у тому, що спікання різнорідних матеріалів (з різними температурами топлення) є складним евтектичним процесом, в якому, поряд із самодифузією, яка зумовлює перенесення маси в область контакту частинок, відбувається взаємна дифузія, що забезпечує гомогенізацію складу шляхом вирівнювання концентрацій різнойменних атомів у межах зразка. В умовах обмеженої розчинности або повної нерозчинности компонентів спікання системи ускладнюється ізолюванням однорідних частинок від взаємного контакту, перешкоджаючи перебігу самодифузії та тим самим погіршуючи умови спікання. Для чисельного розв'язування задачі використано методу Рунґе–Кутти четвертого порядку точности зі змінним кроком інтеґрування. Розроблено програмний комплекс розв'язання задачі, а результати розрахунку наведено на прикладі стопу порошкової суміші заліза, чавуну та ситалізованого скла.

Ключові слова: металокерамічні та металоскляні матеріали, твердофазове та рідкофазове спікання, само- та взаємна дифузія, реологія спікання.

Т. Г. Джаббаров, О. А. Дышин, М. Б. Бабанлы, И. И. Аббасов
Кафедра машиностроения и материаловедения,
Азербайджанский государственный университет нефти и промышленности,
просп. Азадлыг, 16/21, 1010 Баку, Азербайджан

МАТЕМАТИЧЕСКОЕ МОДЕЛИРОВАНИЕ ПРОЦЕССА СПЕКАНИЯ МЕТАЛЛОСТЕКЛЯННЫХ МАТЕРИАЛОВ НА ОСНОВЕ ЖЕЛЕЗА

На основе исследования механизмов диффузионной коалесценции и коагуляции обозреваются математические методы описания и построения моделей процесса спекания металлокерамических материалов. Эти модели представлены системой нелинейных дифференциальных уравнений, включающих коэффициенты объёмной, зернограничной и поверхностной диффузии, а также соответствуют последовательности стадийных уровней температуры, возрастающих с определённой скоростью и имеющих разные продолжительности. Регулируя уровни, скорости и продолжительности температурных режимов, технические параметры шихты, можно контролировать процесс спекания в режиме онлайн. Описание кинетики жидкофазного спекания под давлением проведено на основе реологической теории спекания с использованием механизма диффузионно-вязкого течения, в соответствии с которым происходит тангенциальное проскальзывание вдоль границ зёрен и уменьшение объёма пор из-за выталкивания вакансий на поверхность. После образования жидкой фазы при спекании порошкового тела (в общем случае) вначале обнаруживается рост зёрен, а затем — усадка получаемого сплава. Процесс спекания порошков железа, чугуна и ситалла рассмотрен как взаимная диффузия двух (квази)бинарных сплавов: чугуна (железо + углерод) и фаялита (железо + ситалл). Расчёт коэффициента взаимной диффузии результирующего сплава проведён по формуле Даркена. Спекание многокомпонентных систем характеризуется рядом особенностей, заключающихся в том, что спекание разнородных материалов (с различными температурами плавления) является сложным эвтектическим процессом, в котором, наряду с самодиффузией, обуславливающей перенос массы в область контакта частиц, происходит взаимная диффузия, обеспечивающая гомогенизацию состава путём выравнивания концентраций разноимённых атомов в пределах образца. В условиях ограниченной растворимости или полной нерастворимости компонентов спекание системы осложняется изолированием однородных частиц от взаимного контакта, препятствуя протеканию самодиффузии и тем самым ухудшая условия спекания. Для численного решения задачи использован метод Рунге–Кутты четвёртого порядка точности с переменным шагом интегрирования. Разработан программный комплекс решения задачи, а результаты расчёта приведены на примере сплава порошковой смеси железа, чугуна и ситаллизованного стекла.

Ключевые слова: металлокерамические и металлостеклянные материалы, твердофазное и жидкофазное спекание, само- и взаимная диффузия, реология спекания.